Hippocampal theta oscillations are modulated by behaviour in the ferret but persist during both locomotion and immobility

Dunn S.L.S.[1,2], Town S.M.[1], Bizley J.K.[1]*, Bendor D.[2]*

* equal senior author contribution

1. Ear Institute, University College London
2. Institute of Behavioural Neuroscience, University College London

Abstract

Theta oscillations are a hallmark of hippocampal activity across mammalian species and play a critical role in many hippocampal models of memory and spatial navigation. To attempt to reconcile the cross-species differences observed in the presence and properties of theta, we recorded hippocampal local field potentials in rats and ferrets during a localisation task designed to vary locomotion and sensory attention. Here we show that theta oscillations occur during locomotion in both the ferret and rat, however during periods of immobility, theta oscillations persisted in the ferret, contrasting starkly with the switch to large irregular activity (LIA) in the rat. Theta during immobility in the ferret was identified as Type 2 theta due to its sensitivity to atropine and was modulated by behavioural state, with the strongest theta observed during reward epochs. These results demonstrate that even under similar behavioural conditions, there is a variable relationship between theta and behavioural state across different species.

Introduction

The hippocampal formation plays a central role in creating a cognitive map, critical for both memory and navigation. Studies in rodents, including the discovery of place[1], grid[2], and head direction[3] cells, have laid the foundation for our understanding of the neural basis of these functions. Hippocampal neurons operate within a framework of several types of oscillatory rhythms, the most dominant being the theta oscillation[4–7]- a rhythmic disinhibition of the network that is observed as a 5-12 Hz sawtooth oscillation in the local field potential (LFP). Disruption of theta in rodents has been shown to impact memory and navigation[8–11], although a theta bypass can partially recover these functions[12]. Theta oscillations are believed to play an important role in organisation of hippocampal activity[13–16] and inter-region coordination[17–19], and are important features of many models of hippocampal function[20–22].

In rats, two types of theta oscillations have been described, each with distinct behavioural correlates and pharmacology[23,24]. Type 1 theta is observed continuously during active locomotor behaviours[25] and is resistant to anticholinergic drugs such as atropine[24,26]. The abundance of Type 1 theta in the rat and its interactions with neuronal spiking[27,28] and higher frequency LFP oscillations[29–32] have resulted in it being well characterised; Type 1 theta is the basis for all spatial/mnemonic functional attributes described above. Type 2 theta is rare in the awake rat and occurs in short bouts during immobility, typically at a lower frequency (4-7 Hz) than Type 1 theta[23–25,33]. Contrary to Type 1 theta, Type 2 theta is sensitive to anticholinergic drugs[24,26,34]. Additionally, Type 2 theta has typically been elicited by noxious stimuli[33,35–37] while also being associated with a number of cognitive processes including arousal/attention[33], sensorimotor integration[38], emotional processing[39],and mnemonic related behaviours[40,41].

Intracranial EEG in epilepsy patients have recently allowed insights into neural activity in the human hippocampus, and the occurrence of theta oscillations has not been consistent with that observed in the rat: human theta does not appear continuously during locomotion, instead

occurring in transient bursts[42,43]. There has also been debate about the frequency of human theta[42,44–46] and it has recently been suggested that there are functionally distinct low and high frequency components of human hippocampal theta[47].

Short bouts of theta activity, like that seen in the human hippocampus, have been described in the bat[48–50] and primate[51–53]. In some of these studies the occurrence of hippocampal theta oscillations was linked to active sensation: in the primate, theta was phase locked to saccades[52]; in the bat, it was found to co-occur with bouts of echolocation[48]. It has not yet been determined whether these oscillatory bouts correspond to Type 1 or Type 2 theta, however they *do not* appear to be directly linked to locomotion. It is worth noting that while bats and primates rely on distal senses (vision and audition), rodents instead rely mainly on proximal senses (whisking and sniffing). Because rodents whisk and sniff continuously at a theta rhythm during locomotion, it is challenging to dissociate whether theta is truly linked to locomotion or active sensation.

The reason for these substantial differences between species is not immediately clear, although ethology likely plays a role. Primates and bats do have vastly different behaviours and sensory strategies to the rat; primates are visual experts and bats can fly and travel faster and for much larger distances than rats.

To investigate the relationship between hippocampal theta and ethology, we studied the hippocampus of the ferret (*Mustela putorios furo*), a predator of the order *Carnivora*, which has a comparable locomotory behaviour to rodents, but a different dominant sensory strategy that is closer to primates. To hunt their prey, ferrets rely on both vision- having approximately twice the visual acuity[54,55] and more developed binocular vision[56,57] than rats, and saccadic activity [58]- and hearing, with superior sound localisation abilities to rodents[59,60].

We recorded the hippocampal LFP from ferrets while they performed a behavioural task designed to independently manipulate locomotion and sensory attention. Parallel experiments were performed in rats, to allow the direct comparison of theta activity under similar

experimental conditions. With this behavioural task we sought to determine whether theta oscillations are present during locomotion in ferrets, and if they share similar locomotor-related modulations with rat theta. Furthermore, we investigated the effect of changing sensory attentional load on the hippocampal LFP, which could potentially be influenced by a species' dominant mode of sensation (e.g. whisking vs. hearing).

Results

LFP recording during behaviour in rats and ferrets

To investigate the prevalence of hippocampal theta across species we recorded hippocampal neural activity from 3 rats (R1, R2, R3) and 3 ferrets (F1, F2, F3) while they performed an approach-to-target localisation task designed to vary locomotion and sensory attentional load (Fig. 1). Rats performed a two-choice task with two peripheral stimuli locations (approx. -60° and 60°; Fig. 1a) while ferrets performed a 5-choice task with stimuli presented at 30° intervals (Fig. 1c). The task structure was identical across species (Fig. 1b); animals initiated a trial by holding a nose-poke at the centre of the arena for a pseudorandom amount of time between 2.5-3.5 seconds. Once triggered, an auditory (A) or visual stimulus (V) was presented in a noisy background at the periphery of the arena. Individual testing sessions contained only auditory or visual trials. To receive reward animals were required to approach the location at which the stimulus was presented. All animals performed above chance in the localisation task for both stimulus modalities (rats Fig. 1d; proportion correct, mean ± standard deviation (S.D.) across sessions A: R1 0.87 ± 0.08, R3 0.90 ± 0.08; rat R2 did not perform any A sessions, see Methods; V: R1 0.94 ± 0.03, R2 0.84 ± 0.09, R3 0.99 ± 0.01; ferrets Fig. 1g; A: F1 0.79 ± 0.15, F2 0.70 ± 0.26, F2 0.83 ± 0.16; V: F1 0.74 ± 0.09, F2 0.72 ± 0.10, F3 0.81 ± 0.09). Both rats and ferrets moved at similar speeds while performing the behavioural task (rats Fig. 1e,f; mean session speeds ± S.D. excluding speeds < 10 cms^{-1} R1 26.6 ± 1.4 cms^{-1}, R2 32.0 ± 2.1 cms^{-1}, R3 31.3 ± 1.6 cms^{-1}; ferrets Fig 1h,i; F1 29.4 ± 1.3 cms^{-1}, F2 28.0 ± 1.2 cms^{-1}, 31.7 ± 2.3 cms^{-1}).

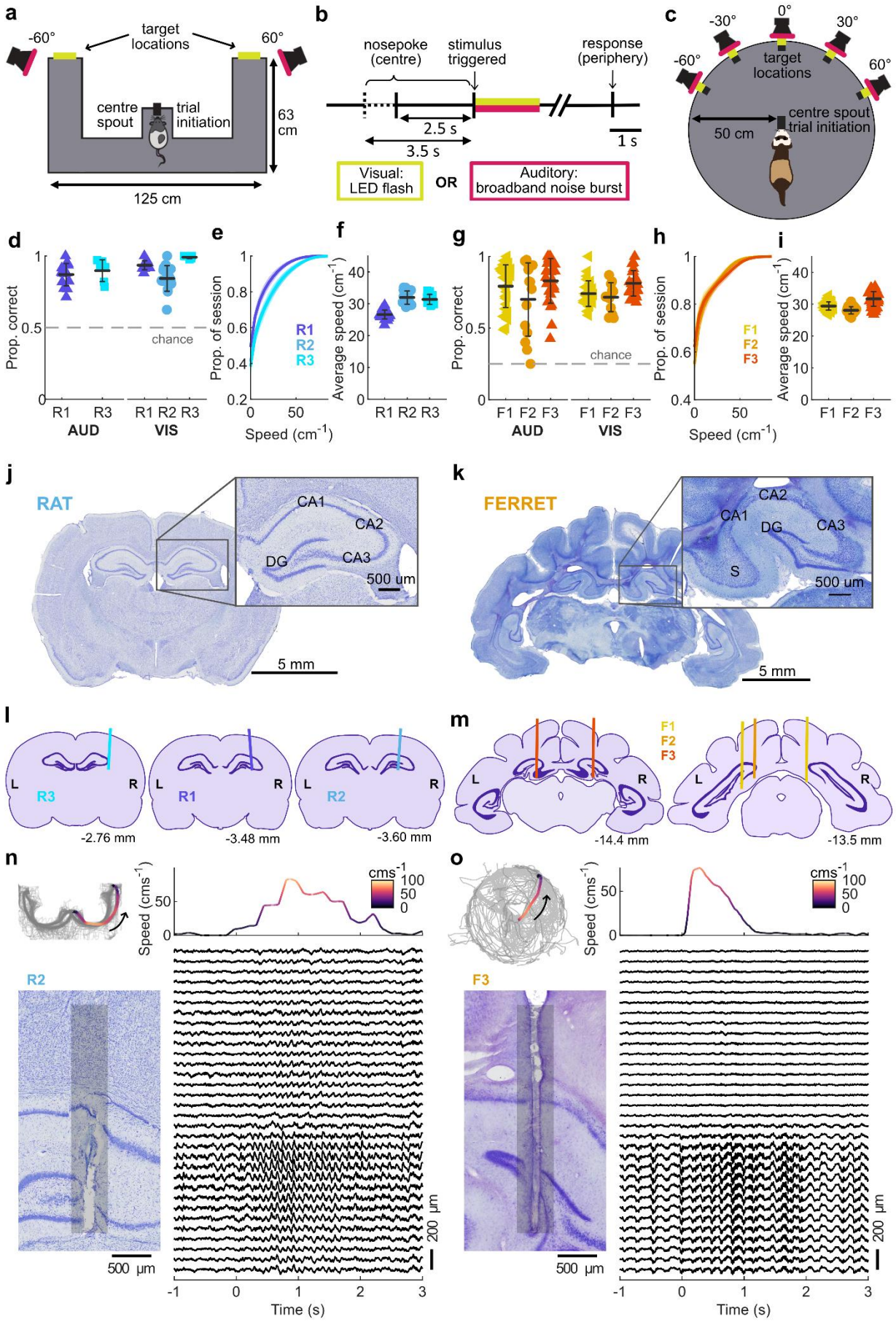
a
-60°
target locations
60°
centre spout
trial initiation
63 cm
125 cm
b
nosepoke (centre)
stimulus triggered
response (periphery)
2.5 s
3.5 s
1 s
Visual: LED flash
OR
Auditory: broadband noise burst
c
-30°
0°
30°
-60°
60°
target locations
centre spout trial initiation
50 cm
d
Prop. correct
chance
R1 R3 R1 R2 R3
AUD VIS
e
Prop. of session
R1
R2
R3
Speed (cm-1)
f
Average speed (cm-1)
R1 R2 R3
g
Prop. correct
chance
F1 F2 F3 F1 F2 F3
AUD VIS
h
Prop. of session
F1
F2
F3
Speed (cm-1)
i
Average speed (cm-1)
F1 F2 F3
j
RAT
CA1
CA2
DG
CA3
500 um
5 mm
k
FERRET
CA2
CA1
DG
CA3
S
500 um
5 mm
l
L
R
R3
R1
R2
-2.76 mm
-3.48 mm
-3.60 mm
m
F1
F2
F3
-14.4 mm
-13.5 mm
n
Speed (cms-1)
cms-1
100
50
0
R2
500 µm
200 µm
Time (s)
o
Speed (cms-1)
cms-1
100
50
0
F3
500 µm
200 µm
Time (s)

Figure 1: LFP recording during behaviour in rats and ferrets.

a-c, Schematics of the behavioural tasks. **a**, Behavioural arena used with rats showing the two peripheral target locations, with the animal holding at the centre initiation spout. **b**, Time-course of the behavioural trial for both the rat and the ferret. **c**, Behavioural arena used with ferrets showing the five peripheral target locations, with the animal holding at the centre initiation spout. **d-i,** Summary of behavioural performance. **d,** Proportion of correct trials for auditory (AUD; left plot; n sessions: R1 16, R3 6; R2 did not perform any AUD sessions, see Methods) and visual (VIS; right plot; n sessions: R1 11, R2 15, R3 7) sessions for each rat. Each marker represents one session, shown with the mean and standard deviation. Grey dashed line represents performance at chance level. **e,** Cumulative speed distribution across sessions for each rat. The mean and standard deviation of the session speed distributions are shown as line and shaded area. **f,** Mean session speed of 'moving' data (i.e. speeds > 10 cms^{-1}) for each rat. Each marker represents one session, shown with the mean and standard deviation. **g,** Proportion of correct trials for auditory (AUD; left plot; n sessions: F1 31, F2 14, F3 24) and visual (VIS; right plot; n sessions: F1 27, F2 12, F3 23) sessions for each ferret. Each marker represents one session, shown with the mean and standard deviation. Grey dashed line represents performance at chance level. **h,** Cumulative speed distribution across sessions for each ferret. The mean and standard deviation of the session speed distributions are shown as line and shaded area. **i,** Mean session speed of 'moving' data (ie speeds > 10 cms^{-1}) for each ferret. Each marker represents one session, shown with the mean and standard deviation. **j-m,** Anatomy of the hippocampal formation and electrode position across species. **j-k,** Nissl stained coronal sections of **j,** the rat (from R1; 40 um thick; -3.12 relative to Bregma) and **k,** the ferret (from F1; 50 um thick; -14.4 mm relative to occipital crest) brain. Insets show magnified images of the dorsal pole of the hippocampal formation. The distinct laminar structure of the hippocampal formation can be seen across species. (CA cornu ammonis, DG dentate gyrus, S subiculum) **i-m,** Summary of electrode implant locations. **l,** Estimated electrode implant locations for each rat. Brain section outlines were generated from the Allen Rat Brain Atlas [ref]. Left (L) and right (R) hemispheres are indicated for each section. The left section is most anterior; the anterior-posterior position of the section is given in millimetres relative to bregma. **m,** Estimated electrode implant locations for each ferret. Brain section outlines were generated from the Ferret Brain Atlas [ref]. Left (L) and right (R) hemispheres are indicated for each section. The left section is most anterior; anterior-posterior position of the section is given in millimetres relative to the occipital crest. **n-o,** Example position and neural data from a single trial, specifically from one second before stimulus onset to three seconds post stimulus onset. **n,** Example trial data from rat R2. *Top left:* Head position tracking of a single recording session (grey line) with a single trial highlighted in a line colour coded by speed. The arrow indicates direction of travel. *Top right:* The speed of the trial highlighted in the head position plot; the same colour coding is used for both position and speed plots. *Bottom left:* Nissl stained section of the hippocampus showing the estimated position of electrode recording sites (grey bar). *Bottom right:* Corresponding LFP trace for the example trial across all channels of the probe (100 um channel spacing). Time at 0 s represents stimulus onset. **o,** Same as **n** but for a trial recorded in ferret F3 from the probe in the right hemisphere ($F3_R$).

During performance of the behavioural task we recorded the local field potential (LFP) from the dorsal hippocampus of rats and the homologous septal pole of the ferret hippocampus using 32 channel linear probes (Neuronexus). The distinct laminar structure of the hippocampal formation is conserved in the ferret (Fig. 1j,k) and 3D models of gross hippocampal anatomy were generated and used to target electrode implantations (SFig 1). We implanted electrodes in the rat in the right hemisphere only (Fig 1l; SFig 1), while ferrets received bilateral electrode implantations (Fig 1m, SFig 1). Most probes entered the hippocampal formation directly (R1, R2, $F1_L$, $F3_L$, $F3_R$), crossing the pyramidal cell layer. The remaining implants (R3, $F1_R$, $F2_L$) did not cross the pyramidal cell layer, however hippocampal LFP oscillations were still detected on all channels (SFig.1). Figures 1n and 1o show typical examples of the data obtained during a single behavioural trial for a rat (R2) and a ferret ($F3_R$) respectively.

Rat-like theta oscillations during locomotion in the ferret hippocampus at 4-7Hz

We first sought to determine whether the ferret hippocampus showed rat-like theta oscillations during locomotion. Theta oscillations in the rat have two important hallmarks- 1) distinct anatomical profiles in which the power increases and the phase shifts while travelling through the hippocampal cell layer[5,26], and 2) correlations of frequency and power with speed/acceleration[61–63]. We first characterised these properties in the rat (Fig. 2 a-f, SFig. 2). Theta oscillations were evident in the rat as a prominent peak between 6-10 Hz in the power spectral density (PSD) of the LFP during locomotion (speed > 10cms^{-1}; Fig. 2a). We used a peak-trough detection method that operated on the theta-filtered trace (4-14 Hz, 500ms order FIR filter) to estimate the instantaneous amplitude, power, phase, and frequency of rat theta oscillations (Fig. 2b). Using these metrics, we quantified the speed-theta relationships: we observed a strong positive correlation between speed and theta frequency (Fig. 2c; $\beta_1 = 2.9 \times 10^{-2}$, $p = 4.1 \times 10^{-4}$, $R^2 = 0.96$) and a weaker negative correlation between speed and theta power (Fig. 2d; $\beta_1 = -1.9 \times 10^{-2}$, $p = 6.3 \times 10^{-3}$, $R^2 = 0.68$) for the example channel with the highest overall LFP power along the probe. We estimated these parameters across every channel of the probe to obtain the theta depth profile; Figure 2f shows the result of this for a single recording session in rat R1. As expected, rat theta showed increased power and a phase shift while travelling through the hippocampal cell layer. Locomotion speed and rat theta frequency were highly positively correlated along all channels. Speed and power were positively correlated along the probe, except in the region of highest theta power close to the dentate gyrus (Fig. 2f; SFig. 2 for data across all sessions/rats).

PSDs of the ferret LFP during locomotion showed a prominent low-frequency peak between 4-7 Hz (Fig. 2g). We filtered the ferret LFP between 2-8 Hz (1 s order FIR) and found depth profiles of power, phase shift, speed-frequency and speed-power relationships that were similar to those in the rat (Fig. 2h-l). Thus we concluded that this low-frequency oscillation in the ferret was equivalent to rodent hippocampal theta. The slope of the speed-theta frequency

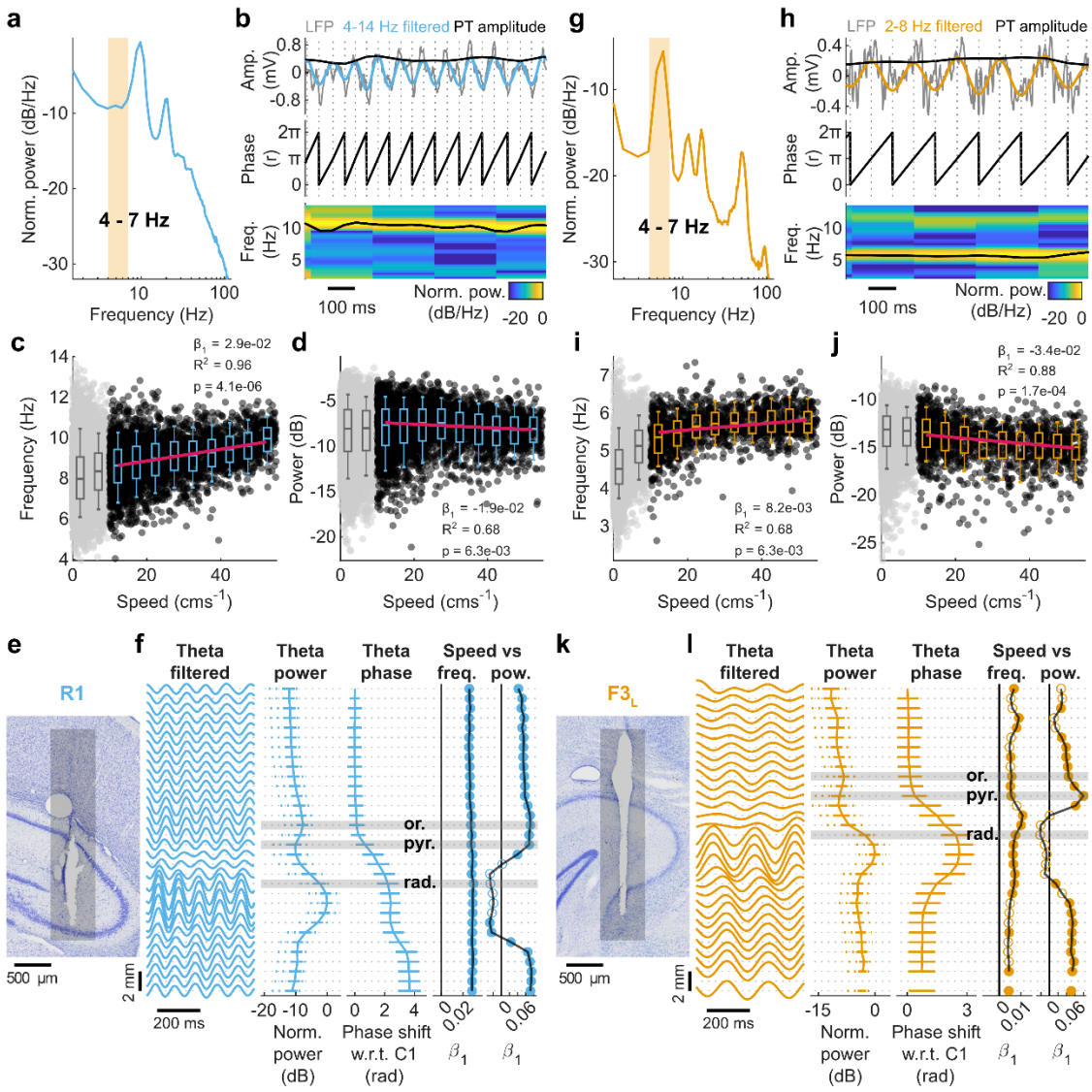

Figure 2: Rat-like theta oscillation in the ferret hippocampus during locomotion occur at 4-7 Hz.

a-d, Measuring theta characteristics in the rat. **a,** Power spectral density of the hippocampal LFP recorded from the channel with highest overall power during locomotion in rat R1 in a single session. Orange shading indicates 4 - 7 Hz range. **b,** Peak-trough method for estimation of instantaneous amplitude, phase, and frequency of theta. *Top:* 1 second example of neural data during locomotion from the same channel and session as shown in **a**. Grey line indicates the LFP (1 Hz highpass filtered). Theta filtered (4-14 Hz) data is shown in blue. Dashed lines indicate positions of extrema detected on the filtered signal used to estimated the theta parameters. The peak-trough amplitude estimate is shown in black. *Middle:* Estimated phase of the filtered signal above. *Bottom:* Estimation of instantaneous frequency (black line) overlaid on spectrogram of the above LFP signal between 2 and 14 Hz. Spectrogram is normalised to maximum. **c-d,** Relationship between locomotor speed and **c,** theta frequency or **d,** theta power for the same channel as shown in **a** for a single recording session. Data points in black represent median values in 250 ms epochs; grey markers show excluded data when the animal was not moving (< 10 cms^{-1}). Box plots show median, interquartile range and 9th to 91st percentile of frequency/power binned by speed (5 cms^{-1} bins). Speeds over the 90th percentile of head speed were excluded (>55 cms^{-1}) due to small sample sizes and are not shown for clarity. Regression line fitted to median values in each speed bin are shown in pink; text shows regression parameters. **e-h,** Measuring theta characteristics in the ferret, same as **a-d** but with data from one recording session of ferret $F3_L$; theta filter bandwidth for the ferret is 2-8 Hz and is shown in orange. **i,** Nissl stained section of the hippocampus of rat R1 showing the estimated electrode track position (grey bar). **j,** Depth profile of theta characteristics for a single recording session of rat R1. *Theta filtered:* LFP signal filtered between 4 and 14 Hz shown for each channel as a function of probe depth. *Theta power:* power profile across the probe. Data shown as medians across probe with interquartile (filled line) and 9th to 91st percentile (dashed) range. *Theta phase:* phase shift for each channel relative to the top channel on the probe. Data shown as circular mean and standard deviation (CircStat Berens, 2009). *Speed vs freq.:* Regression slope of locomotion speed and theta frequency across the probe. *Speed vs pow.:* Regression slope of locomotion speed and theta frequency across the probe. Filled markers indicate significant regressions (Bonferroni corrected $p < 0.0016$), unfilled markers indicate non-significant correlations. Estimated position of hippocampal layers based on theta depth profiles shown with grey shading (stratum oriens, or.; stratum pyramidale, pyr., stratum radiatum, rad.) **k,** Nissl stained section of the hippocampus of ferret $F3_L$ showing the estimated electrode track position (grey bar). **k,** As in **j** but showing depth profile of theta characteristics (filtered 2-8 Hz) for a single recording session of ferret $F3_L$.

relationship was consistently positive for both species, although half that in the ferret compared to the rat (Fig. 2e vs Fig. 2l *Speed vs freq.*).

The depth profiles of these theta properties were heavily influenced by probe position in both species. Supplementary Figure 2 shows the theta depth profiles across all sessions for each individual probe. Only probes that entered the hippocampal formation directly and crossed through the cell layer and apical dendrites show the modulation of theta power, phase, and speed-power correlation with depth as seen in Figure 2.

To group data across varied implant locations we used histological images and the properties of theta oscillations along the probe to estimate the anatomical location of electrodes along the probe to be used for further analysis (Fig. 2e,l, SFig. 2). The pyramidal cell layer (pyr.) was defined by a dip in theta power and the beginning of the theta phase shift. In the rat we confirmed the position of the cell layer using the ripple power (SFig. 2). As theta oscillations have relatively low power in the pyramidal cell layer, we estimated the location of the stratum oriens (or.) and, where appropriate, the stratum radiatum (rad.) along each probe. In probes that crossed the pyramidal cell layer and thus showed theta modulation the stratum oriens and stratum radiatum were determined based on distance from the cell layer. In probes that did not show theta modulation, the stratum oriens channel was typically chosen as the channel with the highest theta power, which also aligned with the estimates of the stratum oriens location from histological data. Channels we estimated to be within the stratum oriens consistently showed positive theta power-speed relationships while those in the stratum radiatum were found to have high theta power, occur below the theta phase shift, and displayed consistent negative speed-power correlation (Fig 2e,l, SFig2).

Low-frequency oscillatory activity persists during immobility in the ferret

Typically, when rats stop moving the LFP transitions from the theta state to large irregular activity (LIA), characterised by a large irregular amplitude and broadband low frequency

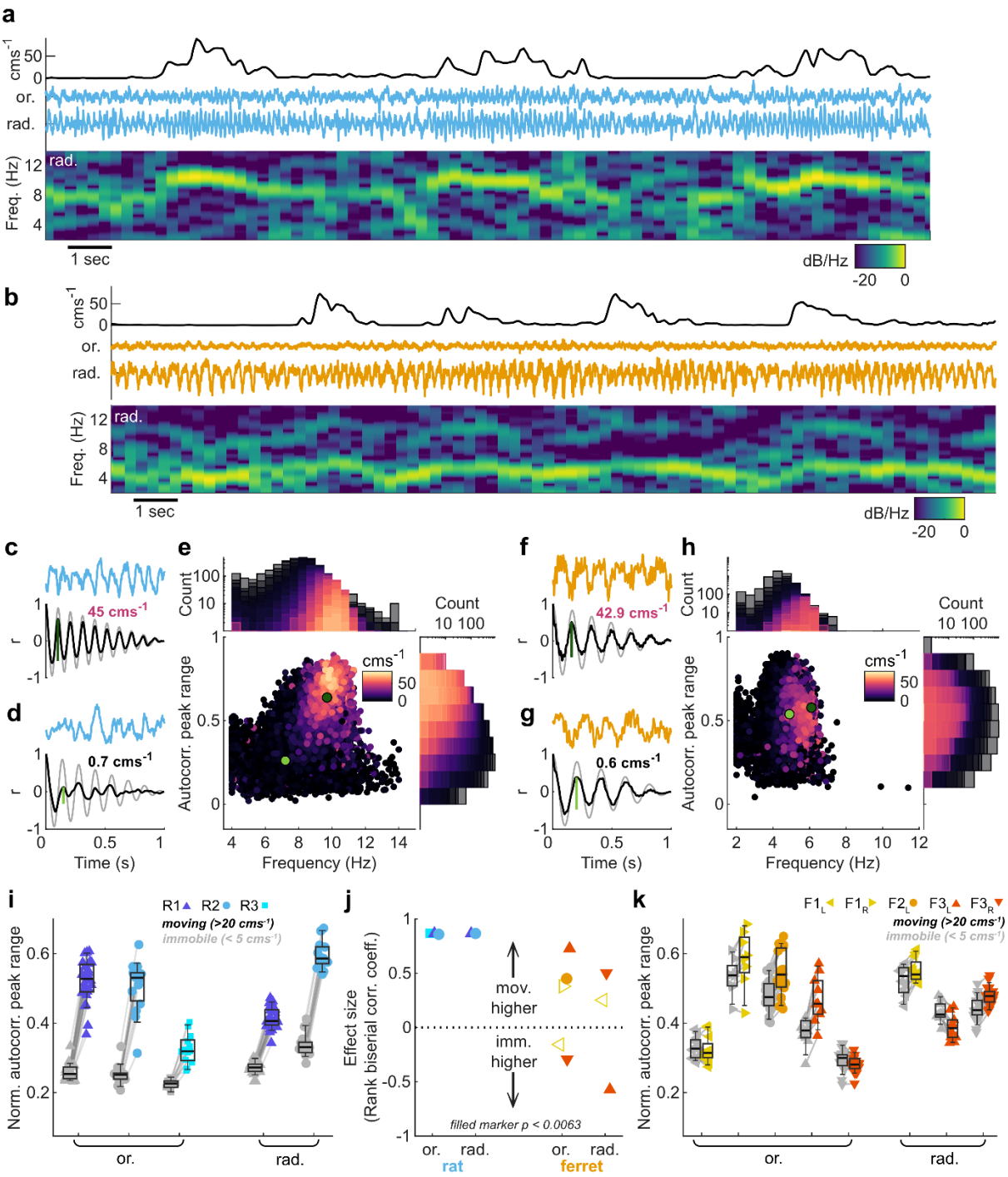

Figure 3: Low frequency oscillatory activity persists during immobility in the ferret hippocampal LFP

a, 20 seconds of example data from rat R2. *Top:* Head speed showing multiple periods of immobility and movement. *Middle:* LFP traces (1 Hz highpass filtered) from stratum oriens (or.) and stratum radiatum (rad.) corresponding to the speed trace above. *Bottom:* Spectrogram between 2-14 Hz of rad. LFP above, normalised to maximum power. Note the bands of high power theta oscillations at 8-10 Hz during locomotion. For clarity the color range was limited to -25 to 0 dB/Hz. **b,** same as in **a** but showing data from ferret $F1_L$. Note the continuous low frequency oscillatory activity during both movement and immobility. **c-d,** Example data segments illustrating the autocorrelation based method of quantifying oscillatory activity. **c,** *Top:* One second example LFP during locomotion from R2 rad. (blue line). The mean head speed in this example epoch is indicated, colour coded by speed as in **e**. *Bottom:* Autocorrelation of the LFP epoch above (black line) overlaid on the matched sine wave autocorrelation (grey line) which is used for frequency estimation and peak range normalisation. Green line indicates the peak range measurement for this example. **d,** same as in **c** but for a data epoch during immobility. **e,** Scatter plot and marginal histograms showing relationship between LFP epoch frequency and normalised autocorrelation peak range for rat R2. Each marker represents a one second data epoch and is colour coded by the mean head speed over the epoch; data are from all sessions. The green markers show the position of the example epochs shown in **c** (moving example, dark green) and **d** (immobile example, light green). **f-h,** same as **c-e** for data from ferret $F1_L$. **i,** Comparison of median normalised autocorrelation peak range for immobile (mean speed < 5 cms^{-1},

grey markers) vs. moving (mean speed > 20 cms^{-1}, blue markers) epochs for each rat (R1 n = 27, R2 n = 15, R3 n = 13 sessions) for data from stratum oriens (or.) and stratum radiatum (rad.). Note that not every probe crossed the stratum radiatum and are thus absent from the plot (see probe implantation summary in Figure 1). Each marker represents data from one recording session, the grey line connects the two locomotor contingencies. Box plots show median, interquartile range and 9th to 91st percentile of session data. **j,** Effect size calculated using the rank biserial correlation coefficient for data shown in **i** (rat data, blue markers) and **k** (ferret data, orange markers) plotted for each probe individually for data from stratum oriens (or.) and stratum radiatum (rad.). Filled markers indicate significant differences between immobile and moving data (sign rank test, Bonferroni corrected $p < 0.0063$), unfilled markers indicate non-significance. Markers used are the same as in **i** and **k**. **k,** as in **i** but for each ferret probe ($F1_L$ n = 12, $F1_R$ n = 8, $F2_L$ n = 23, $F3_L$ n = 10, $F3_R$ n = 22 sessions).

activity (Fig. 3a). However, in the ferret, we observed robust low-frequency oscillatory activity regardless of the locomotor state of the animal (Fig. 3b). When identifying periods of theta oscillations in the rat, the delta-theta power ratio is often used to distinguish theta from high power periods of LIA, however the low frequency range of the ferret meant we were unable to use this method. Therefore to quantify the oscillatory activity we used a metric designed to measure the regularity of an oscillatory signal by parameterising autocorrelograms of LFP epochs. We first segmented the neural traces (high pass filtered, 50 Hz notch filtered) into 1 second epochs and calculated the autocorrelations of each segment (see Fig 3c,d,f,g for examples). For each data epoch we then calculated the Euclidean distance of the epoch autocorrelogram to the autocorrelations of sine waves of varying frequency (4-14 Hz for the rat, 2-14 Hz for the ferret, 0.1 Hz increments). The ‘matched’ sine wave autocorrelogram, i.e. with the minimum Euclidean distance from the epoch autocorrelogram, was used to identify the first autocorrelogram peak and the range of this peak was measured (green lines in Fig. 3c,d,f,g). This peak range measurement was then normalised by the peak range of the matched sine. The frequency of the signal in the data epoch was estimated as the frequency of the matched sine wave. We also segmented the head speed signal into corresponding 1 second epochs and found the mean speed for each epoch. In the rat, at high locomotor speeds, theta oscillatory activity was reflected in the high values for the autocorrelation peak range with frequencies between ~8-10 Hz (Fig. 3c,e). In contrast, at low speeds the autocorrelograms were typically flatter, and thus the peak range lower, and at a broader range of frequencies (Fig. 3d,e), as would be expected for LIA. In the rat, significantly higher peak range values during locomotion than immobility was consistent across animals for theta

recorded in both the stratum oriens and radiatum (Fig 3i,j; Wilcoxon sign rank test, p values range from 5.6 x 10^{-6} to 2.4 x 10^{-4}, rank biserial correlation coefficient effect size range 0.86-0.87). In the ferret however the results were more complex (Fig. 3j,k). Two of the probes, both of which crossed the pyramidal cell layer, showed low peak range values in the stratum oriens during locomotion (Fig 3k; $F1_L$, $F3_R$), and showed either no change ($F1_L$ p = 0.27, effect size = -0.16) or significant increase during immobility ($F3_R$ p = 4.5 x 10^{-3}, effect size = -0.29). The remaining ferret probes showed either no significant change ($F1_R$ p = 0.016, effect size = 0.38), or a significant increase in peak range during locomotion compared to immobility ($F2_L$ p = 4.0 x 10^{-5}, $F3_L$ p = 2.0 x 10^{-3}, effect size 0.73), albeit with a consistently lower effect size than observed in the rat (Fig 3i,j,k). Signals recorded from the ferret stratum radiatum showed either a small increase during locomotion ($F3_L$ p = 2.0 x 10^{-3}, effect size = -0.57), no change in peak range across movement contingencies ($F1_L$ p = 0.016, effect size = 0.25) or a significant increase in peak range during immobility ($F3_R$ p = 5.4 x 10^{-4}, effect size = -0.50). These data indicate that while theta oscillations generally disappear during immobility in the rat, they persist throughout immobile periods in the ferret.

Immobility-related oscillatory activity in the ferret is abolished by atropine

Next, we sought to determine whether this oscillatory activity during immobility in the ferret was Type 2 theta and thus sensitive to the anticholinergic drug atropine. An additional ferret (F4) with a tetrode microdrive positioned in the hippocampus was included in these experiments. Two ferrets (F1, F4) were given I.P. atropine sulphate prior to recording.

We estimated the position of the tetrodes in F4 using the theta power-speed relationship (SFig. 4) and illustrate two channels from the tetrode drive in Figure 4: one estimated to be near the cell layer ($F4_{periCL}$ with a consistently positive theta power-speed relationship) and another estimated to be below the cell layer ($F4_{subCL}$ with a consistently negative theta power-speed relationship). Figure 4a shows example data from ferret F4 from a channel we estimated to

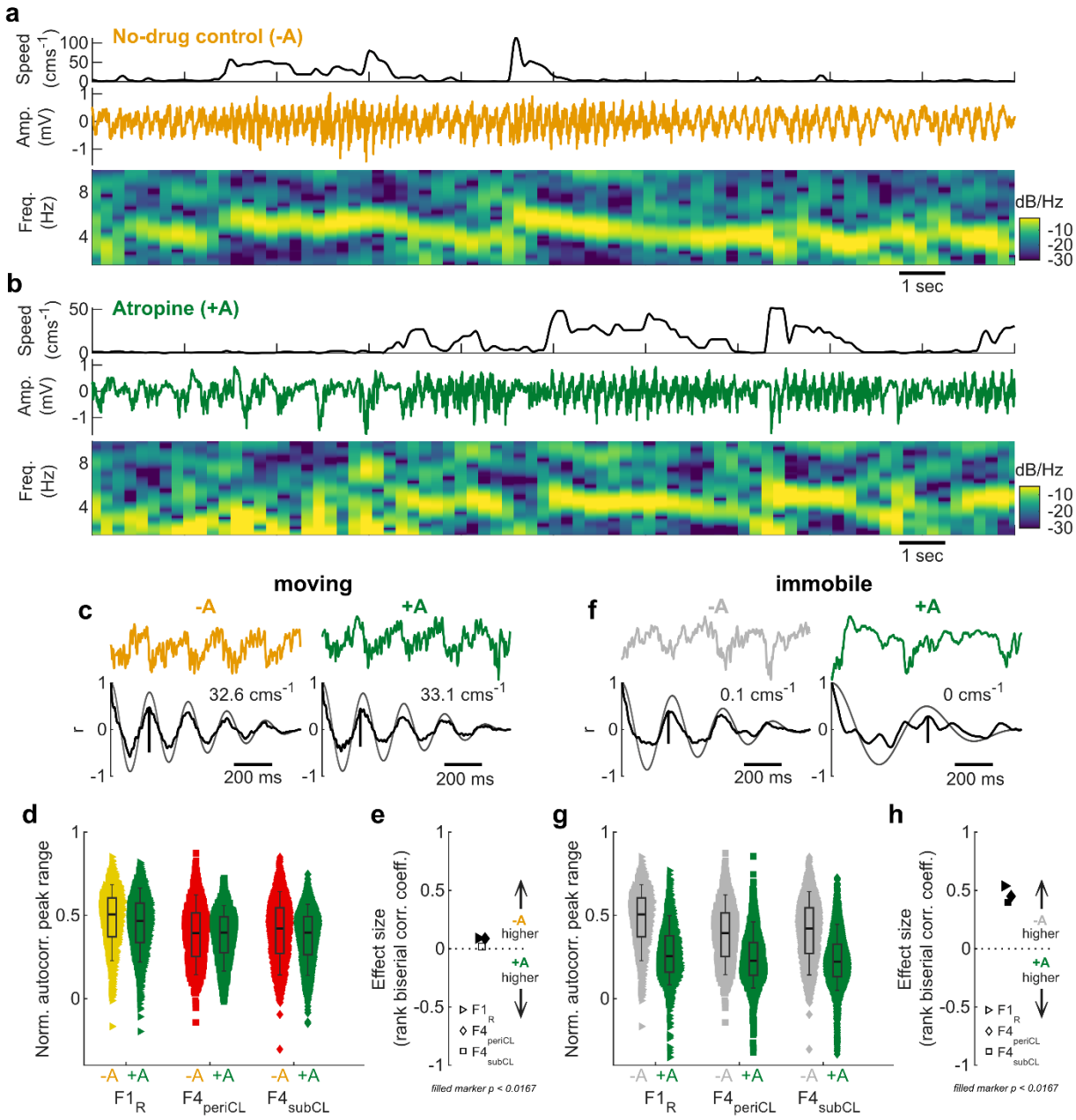

Figure 4: Immobility-related oscillatory activity in the ferret is abolished by atropine

a, 20 seconds of example data from ferret F4 in a control session where no atropine was administered (No-drug control, -A). *Top:* Head speed showing multiple periods of immobility and movement. *Middle:* LFP trace (1 Hz highpass filtered, 50Hz notch filtered) from a channel estimated to be below the cell layer. *Bottom:* Spectrogram between 1.5-10 Hz of LFP above, normalised to maximum power. For clarity the color range was limited to -30 to -2 dB/Hz. **b,** same as in **a** but showing data in a session where atropine was administered (+A). **c-e,** Quantification of theta oscillations during locomotion (> 20 cms^{-1}). **c,** Examples of autocorrelation metric during locomotion without (-A) and with (+A) administration of atropine *Top:* One second example LFPs during locomotion from F4 without (orange line) and with (green line) the administration of atropine. The mean head speed in the example epochs are indicated. *Bottom:* Corresponding autocorrelograms of the LFP epochs above (black line) overlaid on the matched sine wave autocorrelograms (grey line). Black vertical line indicates the peak range measurement for these examples.. **d,** Comparison of median normalised autocorrelation peak range for data during locomotion (mean speed >20 cms^{-1}) without (-A, yellow/red) and with (+A, green) atropine for 3 channels across 2 ferrets. Each marker represents a 1 second data epoch ($F1_R$ n_{-A} = 680, data from 3 sessions, n_{+A} = 662, data from 3 sessions; $F4_{periCL}$ n_{-A} = 783, data from 2 sessions, n_{+A} = 866, data from 2 sessions; $F4_{subCL}$ n_{-A} = 1690, data from 5 sessions, n_{+A} = 2121, data from 5 sessions). Box plots show median, interquartile range and 9th to 91st percentile. **e,** Effect size calculated using the rank biserial correlation coefficient for data shown in **d.** Filled markers indicate significant differences between immobile and moving data (Wilcoxon rank sum test, Bonferroni corrected $p < 0.00167$), unfilled markers indicate non-significance. **f-h** as in **c-e** but with data during immobility (mean speed <5 cms^{-1}).

be below the cell layer during a drug-free control session. Again, robust oscillatory activity was observed in the LFP regardless of movement. In the atropine session, we found that theta oscillatory activity during movement was maintained (Fig 4b-d): two sites showed small but significant increase in the control condition (moving epochs with mean speed >20 cms^{-1} control vs. atropine Wilcoxon rank sum test; $F1_R$ $p = 4.7 \times 10^{-5}$, effect size = 0.090; $F4_{subCL}$ $p = 3.1 \times 10^{-10}$, effect size = 0.087), while the third showed no significant change across the control and atropine sessions ($F4_{periCL}$ p = 0.38, effect size = 0.0185). Oscillatory activity during immobility was abolished; we found significant decreases in autocorrelogram peak ranges during immobility in the atropine sessions compared to control (Fig 4b,f-h; immobile epochs mean speed >5 cms^{-1} control vs. atropine $F1_R$ $p = 4.5 \times 10^{-132}$, effect size = 0.54; $F4_{periCL}$ $p = 4.5 \times 10^{-78}$, effect size = 0.40; $F4_{subCL}$ $p = 6.8 \times 10^{-231}$, effect size = 0.45). These effects were largely consistent across all channels recorded (SFig. 4).

Type 2 theta in the ferret is modulated by behavioural state

Following our classification of Type 1 and Type 2 theta, we next explored how these may be modulated during the behavioural task. We selected 3 epochs of interest (Fig. 5a,f): when the animals were holding at the centre spout to initiate a trial (Hold); locomotion to the goal location (Run); and when the animals were receiving reward (Reward). Autocorrelograms were calculated for each epoch and we measured the peak range as before to quantify the theta oscillations (Fig. 5b,g). Figure 5c-d illustrates the increase in peak range for Run epochs over Hold and Reward for all trials of rat R1 in the stratum radiation (Fig 5c) and across all channels (Fig 5d). Run values were consistently higher than Hold and Reward epochs for all rats, in both the stratum oriens and stratum radiatum (Fig. 5e, Wilcoxon sign rank test, p value min-max range 9.0×10^{-169} to 4.6×10^{-27}, effect size -0.48 to -0.84; SFig 5). Surprisingly, in the ferret's stratum radiatum we found that Reward epochs were higher than both Run and Hold, as illustrated for all trials in $F3_L$ (Fig. 5h,i) and across all radiatum channels (Fig. 5j, Run vs

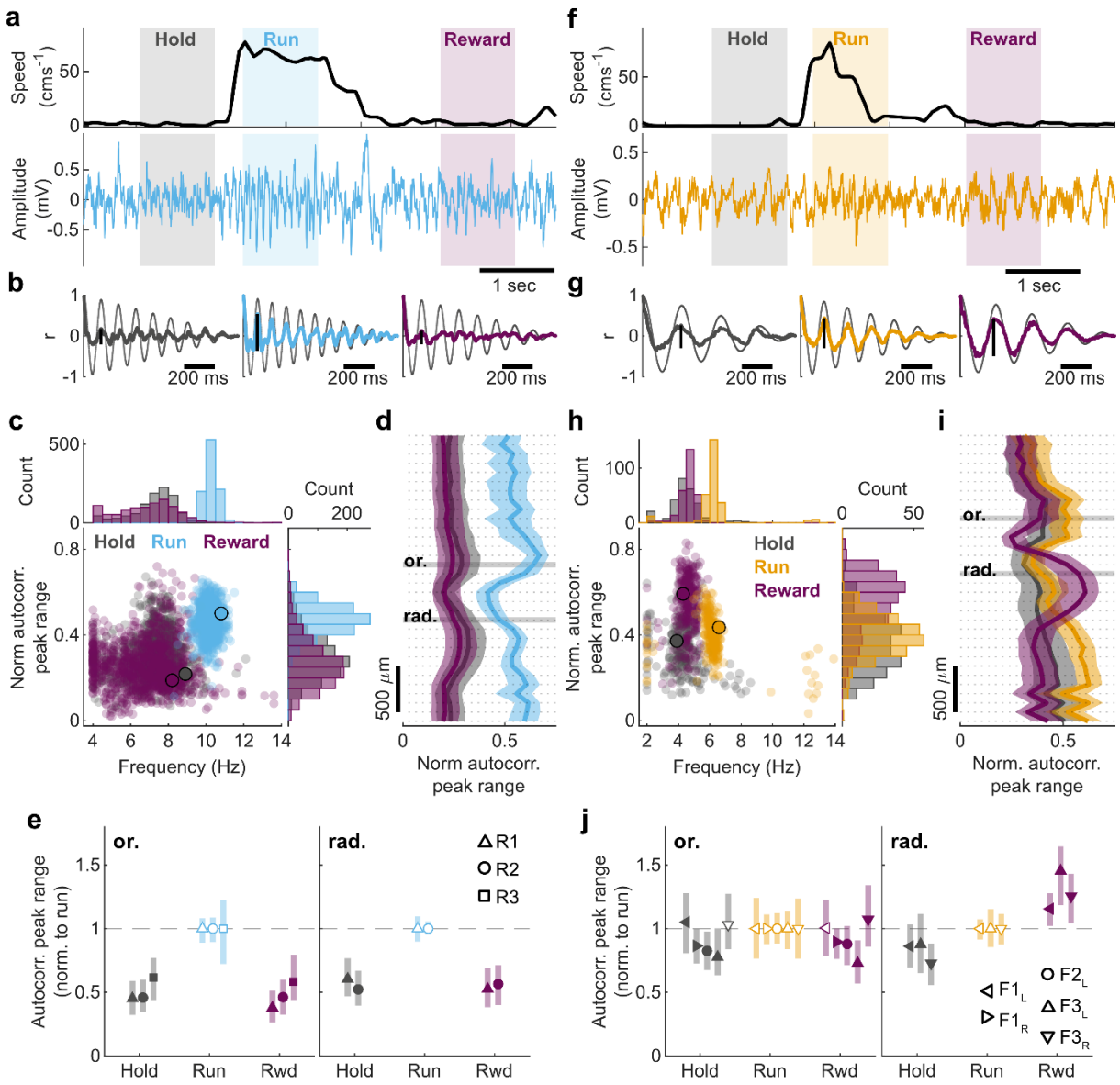

Figure 5: Type 2 theta in the ferret is modulated by behavioural state

a-d, Quantification of oscillatory activity during behaviour in rat R1. **a,** *Top:* Head speed across a single example trial with Hold (grey shading), Run (blue shading), and Reward (purple shading) epochs highlighted. *Bottom:* Corresponding neural trace (2 Hz high pass filtered, 50 Hz notch filtered) recorded from the stratum radiatum of rat R1. **b,** Autocorrelograms of the LFP segments during the trial epochs highlighted in **a:** Hold (grey, *left plot*), Run (blue, *middle plot*), Reward (purple, *right plot*); overlaid on the matched sine wave autocorrelation (light grey lines). The black vertical lines illustrate the peak range measurement for each epoch. **C,** Scatter plot and marginal histograms showing relationship between LFP trial epoch frequency and normalised autocorrelation peak range for Hold (grey), Run (blue), and Reward (purple) epochs in rat R1. Each marker represents data from a one second epoch from a single trial; data are from all sessions. The markers edged with black show the position of the example epochs shown in **b**. **d,** Normalised autocorrelation peak range for Hold (grey), Run (blue), and Reward (purple) epochs across all probe channels for rat R1; data are from all sessions and are presented as median (solid line) and interquartile range (shaded area). Channels in the stratum oriens (or.) and stratum radiatum (rad.) are highlighted with horizontal light grey shading. **e,** Normalised autocorrelation peak range for Hold (grey), Run (blue), and Rwd (reward; purple) epochs for each rat (R1 n = 1081, R2 n = 368, R3 = 427 trials) in the stratum oriens (or., *left plot*) and stratum radiatum (rad., *right plot*). Data are presented as median (marker position) and interquartile range (solid line) and normalised to the median Run value; data are from all sessions. Filled marker represents significant difference from Run ($p<0.0019$ sign rank test). **f-i,** as in **a-d** but for ferret $F3_L$; here LFP is 1 Hz high pass filtered and 50 Hz notch filtered. **j,** as in **e** but for ferret probes ($F1_L$ n = 430, $F1_R$ n = 236, $F2_L$ n = 421, $F3_L$ n = 272, $F3_R$ n = 682 trials). For **g-j** ferret Run data are presented in orange.

Rwd p value min-max range 5.8 x 10^{-49} to 6.2 x 10^{-30}, effect size 0.42 to 0.56; SFig 5). Hold epochs were consistently lower than Run in the ferret stratum radiatum (Run vs Hold p value min-max range 4.6 x 10^{-64} to 1.8 x 10^{-5}, effect size -0.51 to -0.20), however the effect size of the difference between Hold and Run was smaller for the ferrets than for the rats. The effect of reward was not observed in the ferret stratum oriens (Fig 5j), 3 of 5 ferret probes showed a small but significant reduction in Reward compared to Run ($F1_R$, $F2_L$ $F3_L$ p value min-max range 3.0 x 10^{-29} to 1.8 x 10^{-12}, effect size -0.50 to -0.28), while another probe showed a small increase in Reward relative to Run ($F3_R$ p = 6.6 x 10^{-7}, effect size= 0.12) and the remaining probe showed no significant difference ($F1_L$ p = 0.39, effect size = 0.02). The Hold values were significantly lower than Run for 3 of 5 ferret stratum oriens channels ($F1_R$, $F2_L$, $F3_L$, p value min-max range 8.6 x 10^{-28} to 3.7 x 10^{-15}, effect size -0.33 to -0.38), again effect sizes were smaller in the ferret than the rat. For the remaining 2 sites in the ferret oriens we found a small significant increase ($F1_L$ p = 1.7 x 10^{-3}, effect size = 0.09) and no significant between Hold and Run ($F3_R$ p = 0.049, effect size 0.063). These data illustrate enhancement of Type 2 theta oscillations during reward epochs in the ferret specific to particular hippocampal layers.

Discussion

Here we provide the first characterisation of theta oscillations in the ferret hippocampus, using parallel behavioural and electrophysiological experiments in rats to provide a direct comparison. In both species, theta was present during locomotion, and possessed similar properties including the relationship of theta frequency with running speed, and a theta phase shift observed passing through the pyramidal cell layer. However, the frequency of theta in the ferret during locomotion (4-7 Hz), was lower than what is typically observed in the rat (5-12 Hz). It has been suggested that the frequency of theta oscillations decreases with brain size across species to facilitate interregional communication across the brain[64]. Our results do not directly contradict this theory however very early studies reported similar theta frequency

bands for theta in the cat[65] and dog[66], species phylogenetically similar to the ferret, but with significantly larger brain sizes. This raises the possibility that species of the same Order or Family share similar hippocampal theta characteristics, rather than simply a direct relationship between theta frequency and brain size.

Recent work has reported respiration-coupled oscillatory activity in the hippocampus of rodents that occur at a similar frequency to, but independently of, theta oscillations[67,68]. While the olfactory system is a dominant sense for ferrets, given their breathing rate is ~0.5 Hz[69], we do not believe that theta is directly tied to a respiratory related signal.

We found a remarkable difference between the behavioural states eliciting theta between the two species in this study. During immobility, robust oscillatory theta activity persisted in the ferret compared to a change from theta to large irregular activity (LIA) in the rat. The sensitivity of this oscillation to atropine, a muscarinic receptor antagonist, gives strong evidence that this oscillatory activity during immobility is equivalent to Type 2 theta described in the rat. The dose of atropine required to abolish Type 2 theta in the ferret (0.6 mg/kg) was considerably lower than previously used in rodents[24,26,34] (25-50 mg/kg), in keeping with the typical dosages of atropine used clinically, as rodents have high levels of atropinase activity. This species difference in the effective dose of atropine may also explain the propensity for oscillatory activity in the ferret hippocampus. Many features of the theta generation network seem to be designed for a propensity to oscillate – membrane oscillations[70], firing resonance[71], and intra-hippocampal network oscillations[72]- and the neuromodulator tone may determine the network state. Thus for the ferret, higher cholinergic tone may result in the hippocampus staying in predominantly an oscillatory state. It may also be the context of the behavioural task that elicits robust Type 2 theta in the ferret, as while we have controlled the context across species we cannot control species-specific arousal levels in response to the behavioural context. Nonetheless, here with the ferret we have found an ideal, new model species for the study of Type 2 theta.

It is not clear why Type 2 theta is so much more prevalent in ferrets compared to rats. Perhaps more surprising is the consequence of persistent theta- the complete absence of LIA (during which sharp wave ripples, and hippocampal replay commonly occur). In rodents, the hippocampus switches between a theta and LIA state, which according to the two-stage model of memory formation[73], is when memory encoding and reactivation occur, respectively. Can Type 2 theta serve a similar function to the LIA state during immobility? Or is it possible that sharp-wave ripples do not occur in the awake ferret, in conflict potentially with the phenomenon of awake replay observed in rodents.

In this study we show behavioural modulation of Type 2 theta in the ferret. Given the link between Type 2 theta and attention/arousal, it would be reasonable to predict increased power of theta oscillations during the hold period as animals are attentive and waiting for the stimulus. However this was not what we observed, rather the Type 2 theta oscillations in the ferret were strongest during receipt of reward. This is also difficult to interpret in the context of theta's relationship with active sensation which may again predict increased theta in the hold time.

Ferrets are a valuable addition to the repertoire of model species in hippocampal research. Their ability to navigate over large home ranges has been shown in feral ferret colonies[74,75]. Personal experience with them has demonstrated their proclivity for exploration; the verb "to ferret" aptly means "to industriously search". Ferrets display prey tracking behaviours - as obligate carnivores they rely on hunting prey to survive- which can be evoked in a laboratory setting[76]. It will be interesting to explore the contribution of the hippocampal formation to these natural behaviours. The ferret is in a phylogenetic branch distinct from the rodent, yet shares many locomotory similarities, and thus these investigations may provide valuable insight into conserved functions of the hippocampal formation.

Methods

Rat Methods

Three adult male Lister Hooded rats were used in this study, during which they performed behavioural tasks and received hippocampal implants for chronic electrophysiological recording. Rats were supplied from Charles River at 250 g at 7 weeks old and were acclimatized for at least one week prior to the onset of behavioural training. Animals were typically housed in groups of 2-4 prior to surgery and then housed individually following electrode implantation. Access to water in the home cage was ad libitum. Access to food in the home cage was ad libitum except during periods of behavioural sessions during which food intake was restricted. During food restriction, rats received a minimum of 15 g of food per day as rewards during testing; if the minimum amount food was not eaten during testing, the remaining food was supplemented at the end of the day. The animals' weight was monitored throughout the course of behavioural training and testing. If animals dropped below 90 % of their target weight they were to be taken off study and given ad libitum access to food. Animals were housed under a 12:12 hr light-dark cycle (lights on 12:30 pm to 11:30 am; dusk 11:30 pm to 12:30 pm; lights off 12:30am to 11:30am; dawn 11:30 am to 12:30 pm).

All rat experimental procedures performed were first approved by a local ethical review committee. Procedures were carried out under license from the UK Home Office in accordance with the Animals (Scientific Procedures) Act 1986.

Rat surgical procedures

Rats were unilaterally implanted with 32 channel linear probes (NeuroNexus, A1x32-Edge-5mm-100-177). Contacts were positioned down the edge of the shank and had 100 µm spacing. Implants were targeted at the right dorsal hippocampus: 2.6 mm lateral and 3.48 mm posterior to Bregma, and were implanted 3.4 mm below the cortical surface.

All surgical tools were sterilized using high temperature steam in an autoclave, or with ethanol where necessary. Aseptic technique was used throughout the surgical procedures. General anaesthesia was initially induced via 3% isofluroane in oxygen in an anaesthetic chamber. Anaesthesia was maintained throughout the surgery with 2% isofluorane in oxygen. Body temperature was maintained at 37 degrees using a heat mat positioned underneath the animal. Animals were held in a stereotaxic frame (DigiW Wireless Digital Stereotaxic frame, Neurostar, Tubingen, Germany) during surgical procedures. An incision was made down the midline to expose the central crest of the skull; retracted skin was held in place with hemostat clamps. The exposed skull was cleaned using a scalpel blade and then hydrogen peroxide. Steriotaxic coordinates were used to mark the position of the craniotomy. Using a high-speed drill (Foredom 1474 micromotor high-speed drill) and a 1.2 mm burr (Fine Science Tools GmbH, Germany), five holes were drilled outside of the marked craniotomy locations into which small stainless steel bone screws were placed. Another screw was inserted into the interparietal bone near the lambdoid suture and was to act as a ground reference for the electrode. A dental adhesive resin cement (Super-Bond, C&B, Sun Medical Company Ldt., Japan) was applied around the five bone screws. The hippocampal craniotomy of approximately 1 mm diameter was then performed with the drill and a 0.7 mm burr (Fine Science Tools GmbH, Germany). A needle was used to make a small hole in the dura at the target implantation region. The electrode was positioned above the exposed cortex using the stereotaxic arm and then carefully inserted into the brain. The craniotomy was then filled with sterile Vaseline, and the implant was built up around the electrode with bone cement (Simplex Rapid, Kemdent, Associated Dental Products Ltd, UK). Once the electrode was initially secured, the ground wire was wrapped around the ground screws. Bone cement was further used to build up the implant, into which the ground wire was embedded. A custom-designed, 3D-printed plastic rail was also secured onto the implant with dental acrylic. Finally, the wound was sutured to obtain a smooth margin around the implant.

Immediately following surgery, animals were closely observed in a heated chamber until the full recovery of motor function, and had been seen to eat and drink. Under veterinary advice, oral administration of meloxicam (0.5mg/ml; Metacam, Norbrook Labs Ldt., UK) was given to the animals for three days following the surgery to reduce inflammation.

Animals were given a 7-day recovery period post-surgery during which they did not perform any behavioural sessions.

Rat histology

Following the completion of recordings rats were administered a terminal overdose of Euthatal (400mg/kg of pentobarbital sodium; Merial Animal Health Ltd, Harlow, UK) prior to transcardial perfusion. For rat R2 electrolytic lesions were performed prior to perfusion using a current generator (A365 Stimulus Isolator, World Precision Instruments, FL, US); a unipolar current of 30 μA was passed through electrodes for 10 s, after which the polarity was reversed and another 10 s of 30 μA current was passed. Pairs of electrodes at the top and tip of the probe were lesioned. During perfusion, the blood vessels were washed with 0.9% saline followed by 400-500 ml 100% formalin. Brains were then extracted and stored in 100% formalin for at least 24 hours. The extracted brains were immersed in a 30% sucrose solution for three days until they sank. Brains were then coronally sectioned at 40 μm using a freezing microtome (Leica CM1850). Every section was stained for Nissl substance to allow the electrode tracks to be observed. Sections were mounted and imaged using an Axio Scan slide scanner (Zeiss).

Rat equipment and data acquisition

Rats were trained and tested in a custom-built sound proof chamber (IAC Acoustics). Within this chamber was a raised track composed of 3 segments: a centre platform and two response arms. The custom-built centre platform was designed to hold an infra-red (IR) sensor (Sharp)

at approximate rat head height. There were two additional IR sensors fixed under the response arms. Reward ports were positioned at the ends of the response arms into which food rewards were dispensed using a pellet dispenser (Campden Instruments Ltd., UK) Light emitting diodes (LEDs; Kingbright Whites) were mounted within a diffusive plastic case above the reward port at the end of the response arms. Loudspeakers were mounted adjacent to the track, positioned to face the centre platform. Stimulus generation and task automation was performed using custom written MATLAB (MathWorks) scripts which communicated with a Tucker-Davis Technologies (TDT) signal processor (RZ6 TDT System 3 processors; Tucker-Davis Technologies, Alachua, FL) and an Arduino Uno. A video camera was installed in the ceiling of the chamber which communicated with the Neuralynx Cheetah processor, allowing for real-time monitoring of the animal during the task. Video data were collected at 25 frames per second.

Rat neural data were recorded during behavioural sessions using a Neuralynx Digital Lynx acquisition system. Voltage signals were recorded at 30 kHz, then digitised and amplified directly on the headstage. Signals were band-pass filtered between 0.1 Hz and 10 kHz and transmitted to a personal computer running Neuralynx Cheetah acquisition software. The behavioural metadata (e.g. stimulus and nose poke times) were also transmitted to the Cheetah acquisition software from the TDT signal processor and the Arduino via TTL pulses sent to the Digital Lynx. A red and green LED were attached to the wireless headstage and the positions of these LEDs were tracked online during recordings with the Neuralynx Cheetah software.

Ferret methods

Four adult female pigmented ferrets (*Mustela putorius furo*) were used in this study, during which they performed behavioural tasks and received hippocampal implants for chronic electrophysiological recording. Ferrets were supplied from Highgate Farm at 7 weeks of age.

Behavioural training began when the animals were at least 16 weeks old and weighed a minimum of 700 g. Animals were typically housed in groups of 2 to 8 and were given ad libitum access to high-protein food pellets; ferrets with free access to water (i.e. not undergoing behavioural testing) were housed in separate groups to those under water restriction (i.e. undergoing behavioural testing). During testing for the behavioural groups, water was removed from the home cage the evening prior to the first testing day; training typically began on Monday, thus water restriction began on Sunday evening. Ad libitum access to water in the home cage was reinstated at the end of a testing run. Testing runs typically lasted 5 days, and so access to water was typically given on Friday evenings. During water restriction ferrets received a minimum of 60 ml/kg of water per day either as water rewards during testing or supplemented as wet food (a mixture of ground high-protein pellets and water) and/or a small volume of water at the end of the day. Animals were weighed daily during behavioural testing to ensure that body weight did not drop below 85 % of the starting weight measured on the first day of the testing run. Animals were housed under a 14:10 hr light-dark cycle in summer (lights on 06:00 to 20:00) and a 10:14 hr light-dark cycle in winter 54 (lights on 08:00 to 18:00). During change over periods the light times were moved by 1 hr per week. All animals underwent regular otoscopic examinations to ensure their ears were clean and healthy.

All ferret experimental procedures performed were first approved by a local ethical review committee. Procedures were carried out under license from the UK Home Office in accordance with the Animals (Scientific Procedures) Act (1986) and PPL 70/7278.

Hippocampal targeting

At the time of this project there was no atlas to guide electrode implantation in the ferret, therefore target positions were estimated prior to the surgeries by constructing three dimensional (3D) reconstructions of 2 ferret brains. Nissl stained coronal sections (50 µm thick, 200 µm spacing) were imaged using a Zeiss AxioScan Z1 slide scanner. Rigid-body

registration was performed using a custom written MATLAB script to align the images. 3D models were then constructed using IMOD, an open source image processing program (Kremer et al., 1996). The 3D models allowed for the gross anatomy of the ferret hippocampus to be visualised. The implantation target was the septal (dorsal) pole of the hippocampus, as the majority of rodent studies have recorded from this region of the hippocampus. Target implant positions in the dorsal hippocampus were visualised in the 3D models and measurements were made with reference to other brain landmarks (Table 1). Due to the unreliable nature of landmarks on the ferret skull (He et al., 2002), and considerable inter-animal variability in the gross anatomical structure of the brain and skull, defining stereotaxic coordinates for hippocampal implantation was best achieved relative to other brain landmarks. As the lab has developed reliable landmarks for exposing the middle ectosylvian gyrus (MEG; 11 mm from midline, 12 mm from back of skull), where the auditory cortex (AC) is located, it was decided that the top of the MEG would serve as a reference landmark for the location of the hippocampal craniotomy. Using the 3D models, measurements of the implant target position were taken with reference to the top of the MEG. The hippocampal implant target was on the lateral gyrus (LG), therefore the midline and the lateral sulcus were chosen as additional reference landmarks to guide the position of the implant. The 3D model was also used to measure the depth on the dorsoventral axis needed to reach the hippocampus from the cortical surface.

Reference location	**Distance (mm)**
Medial from MEG	6.6 ± 1.0
Dorsal from MEG	4.6 ± 0.4
Rostral from MEG	2.3 ± 0.3
Lateral from midline	3.3 ± 0.2
Medial from LG	1.8 ± 0.3
Depth of cell layer below cortical surface	5.4 ± 0.3

Table 1: Measurements from 3D model of ferret brain for electrode implant target. Distance is reported as mean ± standard deviation, n = 4.

Ferret surgical procedures

All surgical tools were sterilized using high temperature steam in an autoclave, via ethylene oxide, or with cold sterilant where necessary. Aseptic technique was used throughout the surgical procedures. A veterinary anaesthetist was present throughout. General anaesthesia was initially induced via an intramuscular injection of medetomidine (Dormitor, 0.022 mg/kg, Pfizer) and ketamine (Ketaset, 5 mg/kg, Fort Dodge Animal Health). Animals were then intubated and ventilated; anaesthesia was maintained throughout the surgery with 1.5 % isofluorane in oxygen. An intravenous (I.V.) line was inserted and a saline solution was continuously infused. Heart rate, end-tidal C02, and body temperature were monitored throughout the surgery. Body temperature was maintained at 37 degrees using a heat mat positioned underneath the animal, which was controlled via closed-loop feedback of the animals body temperature. Animals were held in a stereotaxic frame Kopf Instruments, USA) during surgical procedures. The area around the midline over the skull was infused with the local anaesthetic bupivacaine (Marcain, AstraZeneca, UK) to reduce autonomic reactions. An incision was made down the midline to expose the central crest of the skull; retracted skin was held in place with hemostat clamps. Unilaterally, a section of temporal muscle was separated from the skull and then removed using electrocautery tongs. The exposed skull was cleaned using 1 % citric acid solution (0.1 g in 10 ml H20) to prevent muscle regrowth, and a dental adhesive resin cement (Super-Bond, C&B, Sun Medical Company Ldt., Japan) was applied. The location of the AC craniotomy was marked on the skull, and as this was used as a reference for the approximate location of the hippocampal craniotomy. Using a DREMEL drill (DREMEL 4000 rotary tool), two holes were drilled outside of the marked craniotomy locations into which small stainless steel bone screws were placed, which both anchored the implant

and provided an electrical ground for the electrodes. To determine the location of the MEG, an AC craniotomy of approximately 3 x 3 mm was performed.

The portion of skull removed was retained in sterile saline; upon localisation of the implantation target with reference to the MEG (see Section 2.3.1), the skull segment was placed back in the AC craniotomy. The hippocampal craniotomy location was marked around the implantation target, and the craniotomy (3 x 3 mm) was then performed. This craniotomy location was mirrored and marked on the other side of the skull for the contralateral implant. A small hole was made in the dura at the target implantation region. The electrode was positioned above the exposed cortex using a micromanipulator and then carefully inserted into the brain. The craniotomy was then filled with a silicone elastomer adhesive (KwiK-Sil, World Precision Instruments, UK), and the implant was built up around the electrode with bone cement (Palacos R+G, Heraeus Medical, UK). Once the electrode was initially secured, the ground wire was wrapped around two of the small screws in the skull, which functioned as reference for the electrode. Bone cement was further used to build up the implant, into which the ground wire was embedded. This procedure was then repeated on the other side of the skull, although no AC craniotomy was performed as the hippocampal craniotomy location was already determined. Once complete, the implant was built up further with bone cement and small metal hooks were embedded, which served to secure the headstage during neural recordings. Excess skin was then removed, and the wound was sutured to obtain a smooth margin around the implant.

Microdrive Implantation

The surgical procedure for implantation of the tetrode microdrive was similar to that outlined above for the linear probes. However, this implant was unilateral due to the large footprint of the microdrive. Upon localisation of the unilateral hippocampal craniotomy in the same manner as described above, the contralateral temporal muscle was retracted. The exposed skull was then cleaned with citric acid, and Super-Bond was applied. Two bone screws were then

inserted into the skull. The drive was then implanted, grounded, and secured in bone cement as detailed above.

Post-operative care

Immediately following surgery, animals were closely observed until the full recovery of motor function and had been seen to eat and drink. Under veterinary advice, post-operative medication was given to the animals for up to 5 days: subcutaneous (S.C.) injections of 0.5 ml/kg buprenorphine (0.3 mg/ml; Vetergesic, Alstoe Animal Health Ldt, UK) for analgesia; oral administration of 0.1 mg/kg meloxicam (0.5mg/ml; Loxicom, Norbrook Labs Ldt., UK) to reduce inflammation; and antibiotics were given as S.C. injections of 0.1 ml/kg amoxicillin (150 mg/ml; Amoxycare, LA). Animals were given a 7-day recovery period post-surgery during which they did not perform any behavioural sessions. Animals were housed singularly for the initial 3-4 days following the surgery and then housed in a pair for the remainder of the recovery period. After the 7-day recovery period, animals were again housed in groups of 2-8, with grouping determined by whether the animals were undergoing behavioural testing (and thus water restriction) or whether they had free access to water.

Ferret histology

Following the completion of recordings ferrets were administered a terminal overdose of Euthatal (400mg/kg of pentobarbital sodium; Merial Animal Health Ltd, Harlow, UK) prior to transcardial perfusion. For ferret implants F2 L, F3 L and F4 L electrolytic lesions were performed prior to perfusion using a current generator (A365 Stimulus Isolator, World Precision Instruments, FL, US); a unipolar current of 30 μA was passed through electrodes for 10 s, after which the polarity was reversed and another 10 s of 30 μA current was passed. In animals with linear probe implants (F2 L and F3 L) pairs of electrodes at the top, middle and tip of the probes were lesioned. For the tetrode animal (F4 L) one wire on each tetrode was lesioned. During perfusion, the blood vessels were washed with 0.9% saline followed by 1.5-

2L 4% paraformaldehyde in 0.1 M phosphate buffer. Brains were then extracted and stored in 4% paraformaldehyde for at least 24 hours. The extracted brains were immersed in a 30% sucrose solution for three days until they sank. Brains were then coronally sectioned at 50 µm using a freezing microtome (Leica CM1850). Every 4th section was stained for Nissl substance to allow the electrode tracks to be observed. Sections were mounted and imaged using an Axio Scan slide scanner (Zeiss).

Ferret equipment and data acquisition

Ferrets were trained and tested in a custom-built sound proof chamber. Within this chamber was a circular arena of 50 cm radius, with walls and ceiling made with strong plastic mesh. In the centre of the arena floor, a perspex spout was mounted at approximate ferret head height onto a plastic platform. The spout was connected to tubing, through which a water reward could be given, and also contained an infra-red (IR) sensor (OB710, TT electronics, UK) to detect nose-pokes. Eleven additional perspex spouts, all with water tubing and IR sensors, were inserted through the wire mesh wall at equidistant locations (30° separation) around the periphery of the arena, with the exception of the position directly behind the centre spout. Light emitting diodes (LEDs; Kingbright White 8 mm) were attached to the back of the spouts in such a way that the perspex spouts acted as waveguides; when the LEDs were active, the spouts themselves emitted light. This LED positioning was implemented to make responding at the spout more intuitive by combining stimuli and response locations. Loudspeakers (Visaton FRS 8) were mounted 3.5 cm behind the arena wall, in line with each spout. For the localisation task only the 5 front spouts were used to allow for direct comparison between auditory and visual trials. Stimulus generation and task automation was performed using custom written MATLAB (MathWorks Inc., Natick, USA) scripts which communicated with Tucker-Davis Technologies (TDT) signal processors (RX8, RS8, RZ2 TDT System 3 processors; Tucker-Davis Technologies, Alachua, FL). Two cameras were installed in the ceiling of the chamber: a webcam, for monitoring of the animal during the task; and a Prosilica

GC650C camera (Allied Vision Technologies) with a wide angle lens (1.8 mm 3.6 mm FL, Varifocal Video Lens, Edmund Optics) which communicated with a TDT RV2 video processor (Tucker-Davis Technologies, Alachua, FL) and allowed us to track red and green LEDs attached to the animal's headstage, and thus the head position of the animal, with high precision (30 frames per second).

Ferret neural data were recorded during behavioural sessions using a wireless recording system (Wirelss-2100-System, Multi Channel Systems GmbH, Germany). Voltage signals were recorded at 20 KHz, then digitised and amplified 100 times directly on the headstage. Signals were band-pass filtered between 0.1 Hz and 10 kHz. Signals were then transmitted to a wireless receiver which communicated with a personal computer running Multi Channel Suite software (Multi Channel Systems GmbH, Germany). The wireless system was synchronised with the TDT signal processors via a TTL pulse sent from the TDT RX8 signal processor to the MCS interface board.

Atropine administration in the ferret

Ferrets F1 and F4 received I.P. injections of atropine sulphate as described below.

Atropine sulphate has been used to abolish Type II theta in the rat (Kramis et al., 1975; Robinson and Vanderwolf, 1978; Lai-Wo Stan Leung, 1985; Buzsaki et al., 1986), rabbit (Kramis et al., 1975), guinea pig (Sainsbury and Montoya, 1984) and cat (Olmstead and Villablanca, 1977). However, no protocol was found for the administration of atropine to investigate the effects on neural signals in the hippocampus of the ferret. Therefore, a protocol was developed based on the previous literature and with consultation of a veterinarian. The most common route of atropine delivery in the literature was intra-peritoneal (I.P.) injection of atropine sulphate. The dose of atropine given in previous studies to rat and guinea pigs was relatively high (25-50 mg/kg) compared to the pre-anaesthetic dose given to ferrets prior to surgery (0.05 mg/kg). Cats received a dose of 1mg/kg (Olmstead and Villablanca, 1977) and

as carnivorans, are phylogenetically closer to ferrets than rats. Therefore, a gradually increasing dose of I.P. atropine sulphate from 0.05 mg/kg to 1mg/kg was administered to the ferrets over the course of several weeks. The impact of atropine administration at each dose on the animals general behaviour was monitored, both within and outside of behavioural testing, using a specifically developed score sheet. A dose of 0.6 mg/kg was found to be effective in manipulating neural activity in the ferret hippocampus. We therefore included only sessions with doses of 0.6 mg/kg and higher for analysis.

For behavioural testing following the administration of atropine, the task was modified with removal of visual stimuli and a reduction of the background illumination level in the testing chamber. Light levels were lowered as atropine is known to cause dilation of pupils, therefore animals may have become abnormally light sensitive. The length of time the animal had to hold its head in place at the centre spout to trigger a trial was also reduced to make trial initiation easier. In some early sessions following atropine administration locomotion was elicited by experimenter interaction with the ferret, in later sessions the animals acclimated to the drug effects and did not need additional motivation for movement.

Common methods

Behavioural training and testing

Behavioural training

Behavioural training procedures for the rat and ferret were broadly similar. Due to equipment and licensing constraints across the two labs in which this work was performed the rats received food reward and the ferrets received water reward. Both reward types were sufficient motivation for the animals to perform the behavioural task.

Rats and ferrets were trained to perform approach-to-target localisation tasks with auditory (A) and visual (V) stimuli. Rats performed a two-choice task with two peripheral stimuli locations

(approx. -60° and 60°) while ferrets performed a 5-choice task with stimuli presented at 30 degree intervals.

The training protocol for rats and ferrets is summarised in Table 2.

Training stage	Rat	Ferret
Pre-training	Association of centre nose-poke spout with reward.	Association of centre nose-poke spout with reward.
Stage 1	Centre nose-poke triggered flashing AV stimuli (250ms duration) which was presented continuously until animals responded correctly. Incorrect response had no effect. Hold time gradually increased 10 - 300 ms. Centre nosepoke gives no direct reward. Correct response consistently rewarded.	Centre nose-poke triggered flashing A or V stimuli (250ms duration) which was presented continuously until animals responded. Incorrect trials triggered noise burst and light flash from all peripheral locations. Hold time gradually increased 500 - 1000 ms. Gradual decrease to zero in centre reward probability. Correct response consistently rewarded.
Stage 2	Unimodal (A or V) stimuli gradually introduced, incorrect response ends trial and triggered 250 ms error sound (10 kHz pure tone) Hold time gradually increased to 2.5 - 3.5 seconds.	Stimulus presented as 2 second single stimulus. Hold time gradually increased to 2.5 - 3.5 seconds.

<u>Behavioural testing</u>

Once trained both rats and ferrets performed approach-to-target localisation tasks. Rats performed a two-choice task with two peripheral stimuli locations (approx. -60° and 60°) while ferrets performed a 5-choice task with stimuli presented at 30 degree intervals. The task structure was identical across species. To trigger a trial the animal was required to hold in a nose-poke at the centre spout for a fixed hold time, the duration of which was pseudorandomly

chosen from 5 possibilities between 2.5 s and 3.5 s. Once triggered, an auditory (A) or visual stimulus (V) was presented in a noisy background at the periphery of the arena. The location and modality of stimulus was pseudorandomly chosen for each trial.

Within a session stimuli presented were unimodal A or V. To receive reward animals were required to approach the location at which the stimulus was presented. Incorrect responses triggered error responses (rat: 250 ms 20 kHz pure tone; ferret: 100 ms sound and light noise burst). For the ferret, in order to prevent biasing their responses to particular spouts, incorrect responses were followed by “correction trials” where the stimulus from the previous trial was repeated until the animal made a correct response. Ferrets could receive up to five correction trials before the trial was aborted and the next trial was initiated. Rats did not receive correction trials. If either species did not respond within 60 s the trial was aborted and the animal was able to trigger the next trial. Aborted trials were excluded from the current analysis because the animals were not engaged with the behavioural task.

During testing the task switched between blocks of easy trials and blocks of hard trials; blocks were 15 trials long. Difficulty was increased by either reducing stimulus duration (“Duration task”) or reducing the signal-to-noise ratio (SNR; “SNR task”). Only one method of increasing difficulty was employed within a session. Difficulty was gradually increased as the animals' performance increased. Within a modality, the easy condition was identical for both Duration and SNR tasks.

Auditory SNR was calculated as the difference between target signal and background noise in dB SPL. Sound level measurements were made using a measuring amplifier (Bruel & Kjær Type 2610). For the ferret, the background noise level was increased to reduce stimulus SNR, while for the rat the A stimulus level was decreased. Visual SNR was calculated as the ratio of the luminous intensity of the target signal to the luminosity of the background signal.

Luminosity measurements were taken using a photometer (Chroma meter CS-100 A). For both species V SNR was reduced by increasing background light level.

All animals were trained on both visual and auditory stimuli, however rat R2 suffered damage to his hearing during implant surgery and therefore was only tested with visual stimuli.

Data cleaning

Position data cleaning

A red and green LED were attached to recording headstages of both species and the positions of these LEDs were tracked. Position data for the rat was tracked online using the Neuralynx Cheetah software. Ferret position data was tracked offline with custom written MATLAB scripts. For both species the tracking data were processed and cleaned offline with custom written MATLAB scripts. Tracking data were cleaned of large reflections using the following constraints: (1) an LED was not permitted to travel over 50 pixels in one frame (2) the two LEDs were required to be within 30-50 pixels of each other (depending on the exact headstage configuration). Linear interpolation was used to fill gaps of less than 660 ms in the data and traces were smoothed using a median filter (width = 5). For the rat, tracking data were excluded when the door to the sound chamber was open, measured through average intensity of the image, and when the LEDs were out of the field of view for > 0.5 s. The average position of the two LEDs was used to estimate the head position of the animal, and subsequently the head speed of the animal.

Neural data cleaning

Neural data were extracted and processed using custom written MATLAB (MathWorks Inc., Natick, USA) scripts. Neural data were downsampled to 1kHz. As large amplitude movement

artefacts and other noise artefacts (due to e.g. wireless signal dropping out, headstage becoming unplugged) were observed during recordings, a cleaning algorithm was implemented to detect and remove noise artefacts. The cleaning algorithm was run over data from each session individually.

Channels were excluded from analysis on the basis of the power spectral density (PSD; calculated using Welch's method) if (1) the power in the theta band was below a certain threshold (< 2 dB for ferrets, <4 dB for rats), or (2) the 50 Hz noise power was too high (5/1.5 times larger than the theta power peak for the rat/ferret respectively). Sessions were excluded if all channels were removed at this stage of cleaning.

Large amplitude movement artefacts and other noise artefacts on the remaining channels were removed using a cleaning algorithm which used the fact that noise artefacts were present on all channels of the probe. The mean amplitude across all channels was found and peaks in this were identified by thresholding. To calculate the noise threshold, the mode of the distribution of mean channel amplitude was found and multiplied by an empirically chosen factor of 10. Identified noise artefacts were then replaced with NaNs. Zeros and saturation points (for digital systems) were also identified and removed.

Further cleaning algorithms were developed for the rat neural data as scratching artefacts were observed that were not always detected with the initial cleaning algorithm. Furthermore, the scratching artefacts occurred within the hippocampal theta range at 8-12 Hz, so accurate removal of these was imperative. During scratching artefacts, power in the 6-13 Hz band was high across all channels of the probe, including the third of recording sites that were positioned in the cortex above the hippocampus. The power in this band was usually much lower on channels 1-10 during clean periods of neural recording. Therefore, for the cleaning of scratching artefacts the following protocol was implemented:

(1) a 1 kHz resampled signal from each channel within a session was filtered between 6-13 Hz using a zero-lag filter (order = 500 ms), and the 6-13 Hz power across the session was found using the Hilbert transform.

(2) the median 6-13 Hz power of channels 1-10 (i.e. cortical recording sites on the top of the probe) across the session was calculated

(3) a power threshold was calculated using the mode of the distribution of median power

(4) sections of the signal where the median 6-13 Hz power for channels 1-10 exceeded the threshold were removed from all channels and replaced with NaNs.

The scratching artefact removal algorithm also identified and removed putative epochs of high-voltage spike-wave (HVS) events as described by Haggerty and Ji (2014). These epochs were characterised by a high amplitude 8 Hz oscillation in the cortex and the hippocampus, with higher power in the cortex than the hippocampus. A smooth power profile across the probe was also observed, suggesting it reflected a biological process as opposed to a noise artefact. The waveform of the observed oscillatory events closely resembled those described for HVS (Haggerty and Ji 2014; data not shown). As the waveform and power profile of these events did not resemble theta oscillations, the epochs were deemed not appropriate for inclusion in the current study and were removed from the signals.

Data Analysis

Theta filter parameters: rat: 4-14 Hz, FIR filter of order 500 ms, FIR filter; ferret: 2-8 Hz, FIR filter of order 1000ms.

<u>Peak-trough detection method</u>

Peak-trough detection has been used before to calculate the instantaneous frequency and phase of theta oscillations (Bellusio et al. 2012). Also recently a toolbox was released to perform cycle by cycle analysis on neural oscillations, which implements peak-trough detection for frequency estimation (Cole and Voytek, 2018).

Here, the instantaneous frequency, phase, and power of the filtered signal was estimated using a custom written peak-trough detection method. A peak-trough detection algorithm was used to estimate the instantaneous frequency, phase, and power of filtered signals. Signals were scanned on a point by point basis searching for extrema within a voltage range. The voltage search range was chosen to be 25 % of the median amplitude of the total signal across the session. The detected extrema were constrained to alternate between peaks and troughs with peaks being positive and troughs negative. Instantaneous frequency was estimated by calculating the mean between the peak frequency (i.e. the inverse of the time between peak) and the trough frequency. Instantaneous amplitude was calculated as the mean of the absolute values of the peak amplitude and the trough amplitude from which the power was calculated. Instantaneous phase was found by setting the peaks at 0 degrees and the troughs at 180 degrees and interpolating the phase between these points.

Determination of hippocampal layers

To group data across varied implant locations, electrode sites in three hippocampal layers were estimated using the depth properties of theta oscillations (Fig. 2, SFig. 2) and histological data. In probes where the hippocampal formation was entered directly, the pyramidal cell layer (pyr.) was defined by a dip in theta power and the beginning of the theta phase shift. In the rat the position of the cell layer was confirmed using the ripple power (SFig. 2). As theta oscillations have relatively low power in the pyramidal cell layer, the location of the stratum oriens (or.) and, where appropriate, the stratum radiatum (rad.) were then estimated. In probes that crossed the pyramidal cell layer, an electrode site 200 µm above the pyramidal cell layer was selected as the stratum oriens. For the estimation of an electrode within the stratum radiatum the distance between the cell layer and the stratum radiatum/lacunosum-moleculare border was measured (which can be clearly observed in Nissl staining) for each probe and used this distance (typically 400 µm) to select a channel for analysis. In probes that did not cross the cell layer, and thus did not show theta modulation, the stratum oriens channel was

typically chosen as the channel with the highest theta power, which also aligned with the estimates of the stratum oriens location from histological data.

Autocorrelation metric of oscillatory activity

The LFP was first high pass filtered (rat 2 Hz, ferret 1Hz) and then 50 Hz notch filtered using IIR filters. The signal was then segmented into 1 second epochs and autocorrelograms were calculated for each epoch. For each data epoch autocorrelogram, the Euclidean distance (ED) to the autocorrelations of sine waves of varying frequency (4-14 Hz for the rat, 2-14 Hz for the ferret, 0.1 Hz increments) was calculated. The ED between the data and the sine autocorrelograms was normalised by the ED of the individual ED of each sine autocorrelogram. The 'matched' sine autocorrelogram, i.e. with the minimum Euclidean distance from the data epoch autocorrelogram, was used to identify the first autocorrelogram peak. The range of this peak was measured from the maxima of the first peak to the average of the two surrounding troughs. This peak range measurement was then normalised by the peak range of the matched sine, as the peak range was found to vary as a function of frequency. The frequency of the signal in the data epoch was estimated as the frequency of the sine wave that was used to calculate the matched sine autocorrelogram.

The head speed signal was also segmented into corresponding 1 second epochs the mean speed was found for each epoch.

For comparison of moving vs. immobile epochs (Figure 3, 4) conservative speed thresholds were chosen to ensure good separation of locomotor contingencies given that speeds were averaged over a 1 second window. The number of moving and immobile epochs were equalised within each session.

Statistical analyses were performed in MATLAB using the Wilcoxon rank sum test (for unpaired data) and the Wilcoxon signed rank test (for paired data). Effect sizes were calculated using the rank biserial correlation coefficient using the Measures of Effect Size Toolbox v1.6.1 (Hentschke and Stuttgen, 2018).

Detection of trial epochs

Hold windows were defined as -1.05 to -0.05 seconds prior to stimulus onset. Run windows were taken as the 1 s prior to peripheral response. Reward windows were defined as the first 1 second window following peripheral response with speed consistently below 5 cm/s. For the rat, reward windows had the additional constraint of being on the maze arm where the peripheral spout was located.

Only correct trials were used for the analysis in Figure 5.

Author Contributions: S.D., J.K.B., and D.B. designed the experiment; S.D. and S.T. collected and analysed data; S.D., S.T., J.K.B., and D.B., wrote and revised the manuscript.

Acknowledgments:

S.D. UCL SenSyt

J.B. Royal Society/Wellcome Sir Henry Dale Fellowship (098418/Z/12/Z), ERC Consolidator award (SOUNDSCENE)

D.B. ERC starter grant (CHIME) and HFSP Young Investigator Award (RGY0067/2016)

We thank Katherine Wood, Gareth Jones, and Huriye Atilgan for assistance with data collection, and the members of the Bizley and Bendor labs for valuable discussion.

References

1. O'Keefe, J. & Dostrovsky, J. The hippocampus as a spatial map. Preliminary evidence from unit activity in the freely-moving rat. *Brain Res.* **34**, 171–175 (1971).

2. Hafting, T., Fyhn, M., Molden, S., Moser, M.-B. & Moser, E. I. Microstructure of a spatial map in the entorhinal cortex. *Nature* **436**, 801–806 (2005).

3. Taube, J. S., Muller, R. U. & Ranck, J. B. *Head-Direction Cells Recorded from the Postsubiculum in Freely Moving Rats. I. Description and Quantitative Analysis*. *The Journal of Neuroscience* http://www.cogsci.ucsd.edu/~sereno/201/readings/08.04-HeadDirCells.pdf (1990).

4. O'Keefe, J. Hippocampus, theta, and spatial memory. *Curr. Opin. Neurobiol.* **3**, 917–924 (1993).

5. Buzsáki, G. Theta oscillations in the hippocampus. *Neuron* **33**, 325–340 (2002).

6. Buzsáki, G. & Moser, E. I. Memory, navigation and theta rhythm in the hippocampal-entorhinal system. *Nature Neuroscience* vol. 16 130–138 (2013).

7. Colgin, L. L. Mechanisms and Functions of Theta Rhythms. *Annu. Rev. Neurosci.* **36**, 295–312 (2013).

8. Winson, J. Loss of hippocampal theta rhythm results in spatial memory deficit in the rat. *Science (80-.).* **201**, 160–163 (1978).

9. Mitchell, S. J., Rawlins, J. N., Steward, O. & Olton, D. S. Medial septal area lesions disrupt theta rhythm and cholinergic staining in medial entorhinal cortex and produce impaired radial arm maze behavior in rats. *J. Neurosci.* **2**, 292–302 (1982).

10. M'Harzi, M. & Jarrard, L. E. Effects of medial and lateral septal lesions on acquisition of a place and cue radial maze task. *Behav. Brain Res.* **49**, 159–165 (1992).

11. Wang, Y., Romani, S., Lustig, B., Leonardo, A. & Pastalkova, E. Theta sequences are essential for internally generated hippocampal firing fields. *Nat. Neurosci.* **18**, 282–288 (2015).

12. McNaughton, N., Ruan, M. & Woodnorth, M. A. Restoring theta-like rhythmicity in rats restores initial learning in the Morris water maze. *Hippocampus* **16**, 1102–1110 (2006).

13. Hasselmo, M. E., Bodelón, C. & Wyble, B. P. A proposed function for hippocampal theta rhythm: Separate phases of encoding and retrieval enhance reversal of prior learning. *Neural Comput.* **14**, 793–817 (2002).

14. Mizuseki, K., Sirota, A., Pastalkova, E. & Buzsáki, G. Theta Oscillations Provide Temporal Windows for Local Circuit Computation in the Entorhinal-Hippocampal Loop. *Neuron* **64**, 267–280 (2009).

15. Jezek, K., Henriksen, E. J., Treves, A., Moser, E. I. & Moser, M. B. Theta-paced flickering between place-cell maps in the hippocampus. *Nature* **478**, 246–249 (2011).

16. Kay, K. *et al.* Constant Sub-second Cycling between Representations of Possible Futures in the Hippocampus. *Cell* **180**, 552-567.e25 (2020).

17. Jones, M. W. & Wilson, M. A. Theta Rhythms Coordinate Hippocampal and Prefrontal Interactions in a Spatial Memory Task. *PLoS Biol.* **3**, e402 (2005).

18. Siapas, A. G., Lubenov, E. V. & Wilson, M. A. Prefrontal phase locking to

hippocampal theta oscillations. *Neuron* **46**, 141–151 (2005).

19. Grion, N., Akrami, A., Zuo, Y., Stella, F. & Diamond, M. E. Coherence between Rat Sensorimotor System and Hippocampus Is Enhanced during Tactile Discrimination. *PLoS Biol.* **14**, e1002384 (2016).

20. Bush, D., Barry, C., Manson, D. & Burgess, N. Using Grid Cells for Navigation. *Neuron* **87**, 507–520 (2015).

21. Lisman, J. E. & Jensen, O. The Theta-Gamma Neural Code. *Neuron* vol. 77 1002–1016 (2013).

22. Hasselmo, M. E. & Stern, C. E. Theta rhythm and the encoding and retrieval of space and time. *NeuroImage* vol. 85 656–666 (2014).

23. Bland, B. H. The physiology and pharmacology of hippocampal formation theta rhythms. *Prog. Neurobiol.* **26**, 1–54 (1986).

24. Kramis, R., Vanderwolf, C. H. & Bland, B. H. Two types of hippocampal rhythmical slow activity in both the rabbit and the rat: Relations to behavior and effects of atropine, diethyl ether, urethane, and pentobarbital. *Exp. Neurol.* **49**, 58–85 (1975).

25. Vanderwolf, C. H. Hippocampal electrical activity and voluntary movement in the rat. *Electroencephalogr. Clin. Neurophysiol.* **26**, 407–418 (1969).

26. Buzsáki, G., Czopf, J., Kondákor, I. & Kellényi, L. Laminar distribution of hippocampal rhythmic slow activity (RSA) in the behaving rat: Current-source density analysis, effects of urethane and atropine. *Brain Res.* **365**, 125–137 (1986).

27. O'Keefe, J. & Recce, M. L. Phase relationship between hippocampal place units and the EEG theta rhythm. *Hippocampus* **3**, 317–330 (1993).

28. Klausberger, T. *et al.* Brain-state- and cell-type-specific firing of hippocampal interneurons in vivo. *Nature* **421**, 844–848 (2003).

29. Bragin, a *et al.* Gamma (40-100 Hz) oscillation in the hippocampus of the behaving rat. *J. Neurosci.* **15**, 47–60 (1995).

30. Colgin, L. L. & Moser, E. I. Hippocampal theta rhythms follow the beat of their own drum. *Nat. Neurosci.* **12**, 1483–1484 (2009).

31. Scheffer-Teixeira, R. *et al.* Theta phase modulates multiple layer-specific oscillations in the CA1 region. *Cereb. Cortex* **22**, 2404–2414 (2012).

32. Belluscio, M. A., Mizuseki, K., Schmidt, R., Kempter, R. & Buzsáki, G. Cross-frequency phase-phase coupling between θ and γ oscillations in the hippocampus. *J. Neurosci.* **32**, 423–35 (2012).

33. Sainsbury, R. S., Heynen, A. & Montoya, C. P. Behavioral correlates of hippocampal type 2 theta in the rat. *Physiol. Behav.* **39**, 513–519 (1987).

34. Lai-Wo Stan Leung. Spectral analysis of hippocampal EEG in the freely moving rat: Effects of centrally active drugs and relations to evoked potentials. *Electroencephalogr. Clin. Neurophysiol.* **60**, 65–77 (1985).

35. Whishaw, I. Q. Hippocampal electroencephalographic activity in the Mongolian gerbil during natural behaviours and wheel running and in the rat during wheel running and conditioned immobility. *Can. J. Psychol.* **26**, 219–239 (1972).

36. Montoya, C. P., Heynen, A. J., Faris, P. D. & Sainsbury, R. S. Modality Specific Type 2 Theta Production in the Immobile Rat. *Behav. Neurosci.* **103**, 106–111 (1989).

37. Seidenbecher, T., Laxmi, T. R., Stork, O. & Pape, H. C. Amygdalar and hippocampal theta rhythm synchronization during fear memory retrieval. *Science (80-.).* **301**, 846–850 (2003).

38. Bland, B. H. & Oddie, S. D. Theta band oscillation and synchrony in the hippocampal formation and associated structures: The case for its role in sensorimotor integration. *Behav. Brain Res.* **127**, 119–136 (2001).

39. Mikulovic, S. *et al.* Ventral hippocampal OLM cells control type 2 theta oscillations and response to predator odor. *Nat. Commun.* **9**, 1–15 (2018).

40. Sato, N. & Sakata, S. Hippocampal theta activity during delayed nonmatching-to-sample performance in rats. *Psychobiology* **27**, 331–340 (1999).

41. MacDonald, C. J., Carrow, S., Place, R. & Eichenbaum, H. Distinct Hippocampal Time Cell Sequences Represent Odor Memories in Immobilized Rats. *J. Neurosci.* **33**, 14607–14616 (2013).

42. M. Aghajan, Z. *et al.* Theta Oscillations in the Human Medial Temporal Lobe during Real-World Ambulatory Movement. *Curr. Biol.* **27**, 3743-3751.e3 (2017).

43. Bush, D. *et al.* Human hippocampal theta power indicates movement onset and distance travelled. *Proc. Natl. Acad. Sci. U. S. A.* **114**, 12297–12302 (2017).

44. Watrous, A. J. *et al.* A Comparative Study of Human and Rat Hippocampal Low-Frequency Oscillations During Spatial Navigation. *Hippocampus* **23**, 656–661 (2013).

45. Jacobs, J. Hippocampal theta oscillations are slower in humans than in rodents: Implications for models of spatial navigation and memory. *Philos. Trans. R. Soc. B Biol. Sci.* **369**, 20130304 (2014).

46. Bohbot, V. D., Copara, M. S., Gotman, J. & Ekstrom, A. D. Low-frequency theta oscillations in the human hippocampus during real-world and virtual navigation. *Nat. Commun.* **8**, 14415 (2017).

47. Goyal, A. *et al.* Functionally distinct high and low theta oscillations in the human hippocampus. *Nat. Commun.* **11**, 2469 (2020).

48. Ulanovsky, N. & Moss, C. F. Hippocampal cellular and network activity in freely moving echolocating bats. *Nat. Neurosci.* **10**, 224–233 (2007).

49. Yartsev, M. M., Witter, M. P. & Ulanovsky, N. Grid cells without theta oscillations in the entorhinal cortex of bats. *Nature* **479**, 103–107 (2011).

50. Yartsev, M. M. & Ulanovsky, N. Representation of three-dimensional space in the hippocampus of flying bats. *Science (80-.).* **340**, 367–372 (2013).

51. Stewart, M. & Fox, S. E. Hippocampal theta activity in monkeys. *Brain Res.* **538**, 59–63 (1991).

52. Jutras, M. J., Fries, P. & Buffalo, E. A. Oscillatory activity in the monkey hippocampus during visual exploration and memory formation. *Proc. Natl. Acad. Sci.* **110**, 13144–13149 (2013).

53. Courellis, H. S. *et al.* Spatial encoding in primate hippocampus during free navigation. *PLoS Biol.* **17**, e3000546 (2019).

54. Srinivasan, S., Carlo, C. N. & Stevens, C. F. Predicting visual acuity from the structure of visual cortex. *Proc. Natl. Acad. Sci. U. S. A.* **112**, 7815–7820 (2015).

55. Veilleux, C. C. & Kirk, E. C. Visual acuity in mammals: Effects of eye size and

ecology. *Brain. Behav. Evol.* **83**, 43–53 (2014).

56. Law, M. I., Zahs, K. R. & Stryker, M. P. *Organization of Primary Visual Cortex (Area 17) in the Ferret*. *THE JOURNAL OF COMPARATIVE NEUROLOGY* vol. 278 (1988).

57. Hein, A., Courjon, J. H., Flandrin, J. M. & Arzi, M. Optokinetic nystagmus in the ferret: including selected comparisons with the cat. *Exp. Brain Res.* **79**, 623–632 (1990).

58. Stitt, I., Zhou, Z. C., Radtke-Schuller, S. & Fröhlich, F. Arousal dependent modulation of thalamo-cortical functional interaction. *Nat. Commun.* **9**, 1–13 (2018).

59. Kavanagh, G. L. & Kelly, J. B. Midline and lateral field sound localization in the albino rat (Rattus norvegicus). *Behav. Neurosci.* **100**, 200–205 (1986).

60. King, A. J. & Parsons, C. H. Improved auditory spatial acuity in visually deprived ferrets. *Eur. J. Neurosci.* **11**, 3945–3956 (1999).

61. McFarland, W. L., Teitelbaum, H. & Hedges, E. K. Relationship between hippocampal theta activity and running speed in the rat. *J. Comp. Physiol. Psychol.* **88**, 324–328 (1975).

62. Sławińska, U. & Kasicki, S. The frequency of rat's hippocampal theta rhythm is related to the speed of locomotion. *Brain Res.* **796**, 327–331 (1998).

63. Kropff, E., Carmichael, J. E., Moser, E. I. & Moser, M. B. Frequency of theta rhythm is controlled by acceleration, but not speed, in running rats. *Neuron* **109**, 1029-1039.e8 (2021).

64. Buzsáki, G., Logothetis, N. & Singer, W. Scaling brain size, keeping timing: Evolutionary preservation of brain rhythms. *Neuron* **80**, 751–764 (2013).

65. Grastyán, E., Lissák, K., Madarász, I. & Donhoffer, H. Hippocampal electrical activity during the development of conditioned reflexes. *Electroencephalogr. Clin. Neurophysiol.* **11**, 409–430 (1959).

66. Arnolds, D. E. A. T., Lopes da Silva, F. H., Aitink, J. W. & Kamp, A. Hippocampal EEG and behaviour in dog. I. Hippocampal EEG correlates of gross motor behaviour. *Electroencephalogr. Clin. Neurophysiol.* **46**, 552–570 (1979).

67. Nguyen Chi, V. *et al.* Hippocampal Respiration-Driven Rhythm Distinct from Theta Oscillations in Awake Mice. *J. Neurosci.* **36**, 162–177 (2016).

68. Lockmann, A. L. V., Laplagne, D. A., Leão, R. N. & Tort, A. B. L. A Respiration-Coupled Rhythm in the Rat Hippocampus Independent of Theta and Slow Oscillations. *J. Neurosci.* **36**, 5338–5352 (2016).

69. *Biology and Diseases of the Ferret*. *Biology and Diseases of the Ferret* (Wiley-Blackwell, 2014). doi:10.1002/9781118782699.

70. Alonso, A. & Llinás, R. R. Subthreshold Na+-dependent theta-like rhythmicity in stellate cells of entorhinal cortex layer II. *Nature* **342**, 175–177 (1989).

71. Zemankovics, R., Káli, S., Paulsen, O., Freund, T. F. & Hájos, N. Differences in subthreshold resonance of hippocampal pyramidal cells and interneurons: The role of h-current and passive membrane characteristics. *J. Physiol.* **588**, 2109–2132 (2010).

72. Goutagny, R., Jackson, J. & Williams, S. Self-generated theta oscillations in the hippocampus. *Nat. Neurosci.* **12**, 1491–1493 (2009).

73. Buzsáki, G. Two-stage model of memory trace formation: A role for 'noisy' brain states. *Neuroscience* **31**, 551–570 (1989).

74. Norbury, G. I., Norbury, D. C. & Heyward, R. P. SPACE USE AND DENNING BEHAVIOUR OF WILD FERRETS AND CATS. *N. Z. J. Ecol.* **22**, 149–159 (1998).

75. Young, J. B. Movement patterns of two New Zealand mustelids: Implications for predator pest management. (Lincoln, 1998).

76. Apfelbach, R. & Wester, U. The quantitative effect of visual and tactile stimuli on the prey-catching behaviour of ferrets (Putorius furo L.). *Behav. Processes* **2**, 187–200 (1977).